Spectral collocation method for free vibration of sandwich plates containing a viscoelastic core

Ming Ji [a,*], Chao Kang [a], Yu Sekiguchi [a], Masanobu Naito [b], Chiaki Sato [a]

[a] *Institute of Innovative Research, Tokyo Institute of Technology, 4259 Nagatsuta cho, Midoriku, Yokohama 226-8501, Japan*
[b] *Research Center for Macromolecules and Biomaterials, National Institute for Materials Science (NIMS), Ibaraki 305-0047, Japan*

ARTICLE INFO

ABSTRACT

Viscoelastic constrained layer damping is a simple and efficient method for reducing noise, vibration, and fatigue in metal structures. In this work, a spectral collocation method utilizing a layer-wise plate theory was established to inspect the vibration characteristics of a sandwich plate with a viscoelastic core. The displacements of each layer satisfied the Mindlin plate theory. The core's transverse shear stress remained constant. The three layers' transverse displacements were assumed to be identical. The displacement fields were reduced to nine variables by utilizing the interfaces' continuity of the displacements. The equations of motion were obtained by utilizing Hamilton's principle. The viscoelastic core's material properties were considered as frequency-dependent. To address the complex eigenvalue problem, an iterative algorithm was used. The theoretical results were compared with published theoretical and experimental data for fully clamped rectangular sandwich plates to validate the proposed method. The modified Oberst beam method was applied by fitting the impulse response function to obtain the adhesive's frequency-dependent storage modulus and loss factor. The natural frequencies and corresponding loss factors of three sandwich plates with different adhesives were measured by conducting impact tests. The numerical results from the present theoretical method agreed well with the measured results.

1. Introduction

Damping is a crucial method for reducing noise and vibration in mechanical, aerospace, and civil engineering applications. Sandwich structures with viscoelastic cores are widely used because the core's shear deformation can cause damping to dissipate the energy [1].

Several theories have been established to model the sandwich structures, including equivalent single-layer [2345], zigzag [6], and layer-wise [789] theories. The equivalent single-layer theory can simplify the modeling the sandwich structures with fewer variables. However, it cannot satisfy the piecewise displacement continuity and accurately represent the shear stress. In the layer-wise theory, each layer has its unique displacement field. At the interface, the displacements are continuous. Di Sciuva [1011] established a piecewise linear function to satisfy the interface's displacement and stress continuities, and implemented it to address dynamic and static issues of a multilayer rectangular plate with simply supported boundaries. Cho *et al.* [12] introduced a layer-wise plate theory to inspect the vibrations of simply supported rectangular laminated plates. A layer-wise theory that takes interlaminar shear stress and displacement continuities into consider to address

the static problem of a laminated plate was established by Lu and Liu [13]. Robbins and Reddy [14] utilized Reddy's layer-wise plate theory to issue a finite element model to estimate a laminated plate's transverse strains along the thickness direction. The analytical solutions were given by Carrera [15] to estimate the flexural deformation of a cross-ply laminated plate with simply supported boundaries. Wang *et al.* [16] solved the fully clamped sandwich plates' vibration based on the Galerkin assumed modes analysis (GAMA) and Kirchhoff thin plate theory. Rao *et al.* [17] provided analytical answers for vibration issues of a cross-ply laminated plate with simply supported boundaries. A layer-wise plate theory was utilized to address the flexural and free vibration problems of clamped sandwich plates by Ferreira *et al.* [18]. A nonlinear zigzag theory was established by Fares and Elmarghany [19] to address static problem of a composite laminated plate. Plagianakos and Saravanos [20] utilized a layer-wise model to estimate the shear stresses along the thickness direction in sandwich plates. Ćetković and Vuksanović [21] used a layer-wise model [14] to examine the vibration and bending of a simply supported sandwich plate. A layer-wise/solid-element model was developed by Li *et al.* [22] to solve the static and dynamic problem of a composite sandwich plate. Bilasse and
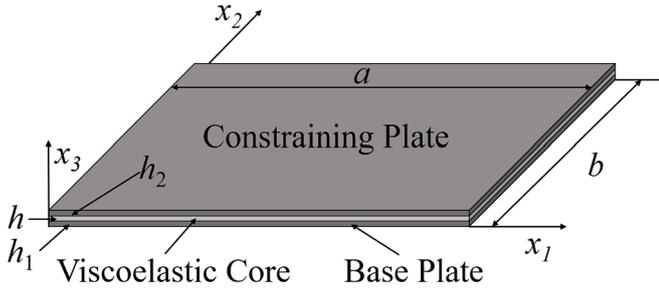
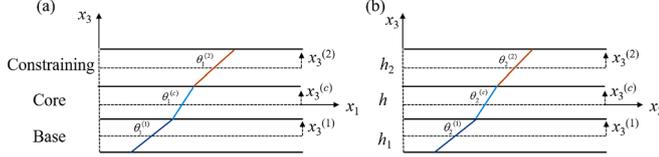---

Fig. 1. Schematic of a sandwich plate.

Fig. 2. Kinetics of first order layer-wise shear deformation in (a) x_1x_3 plane and (b) x_2x_3 plane.

Oguamanam [23] introduced a reduction method addressing forced harmonic vibration of a sandwich plate containing a viscoelastic core. Maturi *et al.* [24] used a new layer-wise theory to handle free vibration and bending of a sandwich plate. A C^0 finite element technique was proposed by Pandey and Pradyumna [25] to address the same problems. An isogeometric method was applied by Liu and Jeffers [26] to deal with the static problems of a functionally graded sandwich plate utilizing Reddy's theory [14]. To handle the free vibration of a sandwich plate in thermal environments, a finite element technique was introduced by Zhao *et al.* [27].

Classical damping models, modern damping models, and the complex modulus method have been utilized to simulate the viscoelastic properties of a structure [28]. Classical damping models involve the Maxwell [23], Kelvin–Voigt [29], and Zener models [3031]. Modern damping models include Fractional Derivatives model [32], Golla–Hughes–McTavish (GHM) method [3334], augmenting thermodynamic fields method [35], and anelastic displacement field (ADF) method [36]. The viscoelastic material properties are known to be dependent on frequency and temperature, which presents challenges in estimating the damping properties of the structure [37]. The Oberst beam method [38] can be applied to measure the viscoelastic material's complex modulus. However, it is only suitable for materials with loss factor significantly larger than that of a base beam. For viscoelastic materials with low loss factor, the base beam's damping must be taken into account.

However, few studies have presented analytical or semi-analytical solutions to address vibration problems of a sandwich plate with high calculation speed and accuracy. The analytical solutions in the aforementioned studies are mostly intended for simply supported plates. The spectral collocation method [39] can accurately and efficiently solve partial differential equations for fluids [404142] and solids [43444546]. A few studies [45] have applied the spectral collocation method to sandwich structures.

Therefore, a spectral collocation method using a layer-wise plate theory was developed to investigate dynamic characteristics of sandwich plates containing viscoelastic cores. The displacements of each layer satisfied the Mindlin plate theory. The core's transverse shear stress remained constant. The three layers' transverse displacements were assumed to be identical. The displacement fields were reduced to nine variables by utilizing the interfaces' continuity of the displacements. Hamilton's principle was applied to obtain the equations of motion. To address the complex eigenvalue problem, an iterative

algorithm was used. The theoretical results were compared with published theoretical and experimental data for fully clamped rectangular sandwich plates to validate the developed method. Then, the modified Oberst beam method was applied by fitting the impulse response function (IRF) to obtain the adhesive's storage modulus and loss factor. The natural frequencies and corresponding loss factors of three sandwich plates with different adhesives were measured by conducting impact tests. The numerical results from the theoretical method agreed well with the measured results.

2. Theoretical formulation

Fig. 1 indicates a sandwich plate containing a viscoelastic core. a was the length, b was the width, h was viscoelastic core's thickness, h_1 was the base plate's thickness and h_2 was the constraining plate's thickness. (x_1, x_2, x_3) was the Cartesian coordinate system. The layer's displacements are

$$u^{(i)}\left(x_1, x_2, x_3^{(i)}, t\right) = u_0^{(i)}(x_1, x_2, t) - x_3^{(i)}\theta_1^{(i)}(x_1, x_2, t) \tag{1}$$

$$v^{(i)}\left(x_1, x_2, x_3^{(i)}, t\right) = v_0^{(i)}(x_1, x_2, t) - x_3^{(i)}\theta_2^{(i)}(x_1, x_2, t) \tag{2}$$

$$w^{(i)}\left(x_1, x_2, x_3^{(i)}, t\right) = w_0(x_1, x_2, t) \tag{3}$$

where θ_1 and θ_2 are the slopes of the normal of the neutral plane; u_0 and v_0 are the in-plane displacements of the neutral plane; index $i = 1$ indicates the base plate, and $i = 2$ denotes the constraining plate; t is time.

The displacements are continuous at the interface between the layers.

$$u^{(2)}\left(x_1, x_2, -\frac{h_2}{2}, t\right) = u^{(c)}\left(x_1, x_2, \frac{h}{2}, t\right), v^{(2)}\left(x_1, x_2, -\frac{h_2}{2}, t\right)$$
$$= v^{(c)}\left(x_1, x_2, \frac{h}{2}, t\right),$$
$$u^{(1)}\left(x_1, x_2, \frac{h_1}{2}, t\right) = u^{(c)}\left(x_1, x_2, -\frac{h}{2}, t\right), v^{(1)}\left(x_1, x_2, \frac{h_1}{2}, t\right)$$
$$= v^{(c)}\left(x_1, x_2, -\frac{h}{2}, t\right). \tag{4}$$

The core's in-plane displacements in the neutral plane are described as

$$u_0^{(c)} = \frac{u_0^{(2)} + u_0^{(1)}}{2} + \frac{h_2\theta_1^{(2)} - h_1\theta_1^{(1)}}{4} \tag{5}$$

$$v_0^{(c)} = \frac{v_0^{(2)} + v_0^{(1)}}{2} + \frac{h_2\theta_2^{(2)} - h_1\theta_2^{(1)}}{4} \tag{6}$$

The rotations of the viscoelastic layer's transverse normal are

$$\theta_1^{(c)} = \frac{u_0^{(2)} - u_0^{(1)}}{h} + \frac{h_2\theta_1^{(2)} + h_1\theta_1^{(1)}}{2h} \tag{7}$$

$$\theta_2^{(c)} = \frac{v_0^{(2)} - v_0^{(1)}}{h} + \frac{h_2\theta_2^{(2)} + h_1\theta_2^{(1)}}{2h} \tag{8}$$

The viscoelastic core's displacements can be rewritten as shown below.

$$u^{(c)}\left(x_1, x_2, x_3^{(c)}, t\right) = \left[\frac{u_0^{(2)} + u_0^{(1)}}{2} + \frac{h_2\theta_1^{(2)} - h_1\theta_1^{(1)}}{4}\right]$$
$$+ x_3^{(c)}\left[\frac{u_0^{(2)} - u_0^{(1)}}{h} + \frac{h_2\theta_1^{(2)} + h_1\theta_1^{(1)}}{2h}\right] \tag{9}$$

$$v^{(c)}\left(x_1, x_2, x_3^{(c)}, t\right) = \left[\frac{v_0^{(2)} + v_0^{(1)}}{2} + \frac{h_2\theta_2^{(2)} - h_1\theta_2^{(1)}}{4}\right]$$
$$+ x_3^{(c)}\left[\frac{v_0^{(2)} - v_0^{(1)}}{h} + \frac{h_2\theta_2^{(2)} + h_1\theta_2^{(1)}}{2h}\right] \tag{10}$$

The kinetics of the first-order layer-wise shear deformation model in x_1x_3 plane and x_2x_3 plane are shown in Fig. 2 (a) and (b), respectively.

The strains of the constraining and base plates are

$$\varepsilon_{11}^{(i)} = \frac{\partial u_0^{(i)}}{\partial x_1} - x_3^{(i)}\frac{\partial \theta_1^{(i)}}{\partial x_1} \tag{11}$$

$$\varepsilon_{22}^{(i)} = \frac{\partial v_0^{(i)}}{\partial x_1} - x_3^{(i)}\frac{\partial \theta_2^{(i)}}{\partial x_1} \tag{12}$$

$$\gamma_{12}^{(i)} = \frac{\partial u_0^{(i)}}{\partial x_2} + \frac{\partial v_0^{(i)}}{\partial x_1} - x_3^{(i)}\left(\frac{\partial \theta_1^{(i)}}{\partial x_2} + \frac{\partial \theta_2^{(i)}}{\partial x_1}\right) \tag{13}$$

$$\gamma_{13}^{(i)} = -\theta_1^{(i)} + \frac{\partial w_0}{\partial x_1} \tag{14}$$

$$\gamma_{23}^{(i)} = -\theta_2^{(i)} + \frac{\partial w_0}{\partial x_2} \tag{15}$$

The shear strains in the core are much larger than the extensional strains. Thus, only the shear strains were considered in the core. The shear strains are

$$\gamma_{13}^{(c)} = \frac{u_0^{(2)} - u_0^{(1)}}{h} + \frac{h_2\theta_1^{(2)} + h_1\theta_1^{(1)}}{2h} + \frac{\partial w_0}{\partial x_1} \tag{16}$$

$$\gamma_{23}^{(c)} = \frac{v_0^{(2)} - v_0^{(1)}}{h} + \frac{h_2\theta_2^{(2)} + h_1\theta_2^{(1)}}{2h} + \frac{\partial w_0}{\partial x_2} \tag{17}$$

The stresses of the constraining and base plates are

$$\sigma_{11}^{(i)} = \left(\varepsilon_{11}^{(i)} + \nu_i\varepsilon_{22}^{(i)}\right)\frac{E_i}{1 - \nu_i^2} \tag{18}$$

$$\sigma_{22}^{(i)} = \left(\varepsilon_{22}^{(i)} + \nu_i\varepsilon_{11}^{(i)}\right)\frac{E_i}{1 - \nu_i^2} \tag{19}$$

$$\sigma_{12}^{(i)} = G_i\gamma_{12}^{(i)} \tag{20}$$

$$\sigma_{13}^{(i)} = \kappa^2 G_i\gamma_{13}^{(i)} \tag{21}$$

$$\sigma_{23}^{(i)} = \kappa^2 G_i\gamma_{23}^{(i)} \tag{22}$$

where κ is the correction factor, $\kappa = \pi/\sqrt{12}$; ν, G and E are Poisson's ratio, shear modulus, and Young's modulus, respectively.

The shear stresses are

$$\sigma_{13}^{(c)} = G_c\gamma_{13}^{(c)} \tag{23}$$

$$\sigma_{23}^{(c)} = G_c\gamma_{23}^{(c)} \tag{24}$$

Hamilton's principle [47484950] were used to derive the equations of motions.

$$\delta T - \delta V = 0 \tag{25}$$

where T is the kinetic energy and V is the potential energy.

$$T = \frac{1}{2}\rho_c\int_0^b\int_0^a\int_{-\frac{h}{2}}^{\frac{h}{2}}\int_0^{t_0}\left((\dot{u}^{(c)})^2 + (\dot{v}^{(c)})^2 + \dot{w}_0^2\right)\mathrm{d}t\mathrm{d}x_3^{(c)}\mathrm{d}x_1\mathrm{d}x_2$$
$$+ \sum_{i=1}^2\frac{1}{2}\rho_i\int_0^b\int_0^a\int_{-\frac{h_i}{2}}^{\frac{h_i}{2}}\int_0^{t_0}\left((\dot{u}^{(i)})^2 + (\dot{v}^{(i)})^2 + \dot{w}_0^2\right)\mathrm{d}t\mathrm{d}x_3^{(i)}\mathrm{d}x_1\mathrm{d}x_2 \tag{26}$$

$$V = \frac{1}{2}\int_0^b\int_0^a\int_{-\frac{h}{2}}^{\frac{h}{2}}\int_0^{t_0}\left(\sigma_{13}^{(c)}\gamma_{13}^{(c)} + \sigma_{23}^{(c)}\gamma_{23}^{(c)}\right)\mathrm{d}t\mathrm{d}x_3^{(c)}\mathrm{d}x_1\mathrm{d}x_2$$
$$+ \sum_{i=1}^2\frac{1}{2}\int_0^b\int_0^a\int_{-\frac{h_i}{2}}^{\frac{h_i}{2}}\int_0^{t_0}\left(\sigma_{11}^{(i)}\varepsilon_{11}^{(i)} + \sigma_{22}^{(i)}\varepsilon_{22}^{(i)} + \sigma_{12}^{(i)}\gamma_{12}^{(i)}\right.$$
$$\left. + \sigma_{13}^{(i)}\gamma_{13}^{(i)} + \sigma_{23}^{(i)}\gamma_{23}^{(i)}\right)\mathrm{d}t\mathrm{d}x_3^{(i)}\mathrm{d}x_1\mathrm{d}x_2 \tag{27}$$

where t_0 is the final time; the "." refers to time derivative. Eq. (25) is established for arbitrary $\delta u_0^{(1)}$, $\delta u_0^{(2)}$, $\delta v_0^{(1)}$, $\delta v_0^{(2)}$, $\delta\theta_1^{(1)}$, $\delta\theta_1^{(2)}$, $\delta\theta_2^{(1)}$, $\delta\theta_2^{(2)}$, and δw_0.

$$\frac{\partial N_{11}^{(1)}}{\partial x_1} + \frac{\partial N_{12}^{(1)}}{\partial x_2} + \frac{N_{13}^{(c)}}{h} =$$
$$\rho_1h_1\ddot{u}_0^{(1)} + \rho_ch\left(\frac{\ddot{u}_0^{(2)}}{6} + \frac{\ddot{u}_0^{(1)}}{3} + \frac{h_2}{12}\ddot{\theta}_1^{(2)} - \frac{h_1}{6}\ddot{\theta}_1^{(1)}\right) \tag{28.a}$$

$$\frac{\partial N_{11}^{(2)}}{\partial x_1} + \frac{\partial N_{12}^{(2)}}{\partial x_2} - \frac{N_{13}^{(c)}}{h} =$$
$$\rho_2h_2\ddot{u}_0^{(2)} + \rho_ch\left(\frac{\ddot{u}_0^{(2)}}{3} + \frac{\ddot{u}_0^{(1)}}{6} + \frac{h_2}{6}\ddot{\theta}_1^{(2)} - \frac{h_1}{12}\ddot{\theta}_1^{(1)}\right) \tag{28.b}$$

$$\frac{\partial N_{12}^{(1)}}{\partial x_1} + \frac{\partial N_{22}^{(1)}}{\partial x_2} + \frac{N_{23}^{(c)}}{h} =$$
$$\rho_1h_1\ddot{v}_0^{(1)} + \rho_ch\left(\frac{\ddot{v}_0^{(2)}}{6} + \frac{\ddot{v}_0^{(1)}}{3} + \frac{h_2}{12}\ddot{\theta}_2^{(2)} - \frac{h_1}{6}\ddot{\theta}_2^{(1)}\right) \tag{28.c}$$

$$\frac{\partial N_{12}^{(2)}}{\partial x_1} + \frac{\partial N_{22}^{(2)}}{\partial x_2} - \frac{N_{23}^{(c)}}{h} =$$
$$\rho_2h_2\ddot{v}_0^{(2)} + \rho_ch\left(\frac{\ddot{v}_0^{(2)}}{3} + \frac{\ddot{v}_0^{(1)}}{6} + \frac{h_2}{6}\ddot{\theta}_2^{(2)} - \frac{h_1}{12}\ddot{\theta}_2^{(1)}\right) \tag{28.d}$$

$$\frac{\partial M_{11}^{(1)}}{\partial x_1} + \frac{\partial M_{12}^{(1)}}{\partial x_2} - N_{13}^{(1)} + \frac{h_1N_{13}^{(c)}}{2h} =$$
$$-\frac{\rho_1h_1^3}{12}\ddot{\phi}_1^{(1)} + \rho_chh_1\left(\frac{\ddot{u}_0^{(2)}}{12} + \frac{\ddot{u}_0^{(1)}}{6} + \frac{h_2}{24}\ddot{\theta}_1^{(2)} - \frac{h_1}{12}\ddot{\theta}_1^{(1)}\right) \tag{28.e}$$

$$\frac{\partial M_{11}^{(2)}}{\partial x_1} + \frac{\partial M_{12}^{(2)}}{\partial x_2} - N_{13}^{(2)} - \frac{h_2N_{13}^{(c)}}{2h} =$$
$$-\frac{\rho_2h_2^3}{12}\ddot{\phi}_1^{(2)} - \rho_chh_2\left(\frac{\ddot{u}_0^{(2)}}{6} + \frac{\ddot{u}_0^{(1)}}{12} + \frac{h_2}{12}\ddot{\theta}_1^{(2)} - \frac{h_1}{24}\ddot{\theta}_1^{(1)}\right) \tag{28.f}$$

$$\frac{\partial M_{12}^{(1)}}{\partial x_1} + \frac{\partial M_{22}^{(1)}}{\partial x_2} - N_{23}^{(1)} + \frac{h_1N_{23}^{(c)}}{2h} =$$
$$-\frac{\rho_1h_1^3}{12}\ddot{\phi}_2^{(1)} + \rho_chh_1\left(\frac{\ddot{v}_0^{(2)}}{12} + \frac{\ddot{v}_0^{(1)}}{6} + \frac{h_2}{24}\ddot{\theta}_2^{(2)} - \frac{h_1}{12}\ddot{\theta}_2^{(1)}\right) \tag{28.g}$$

$$\frac{\partial M_{12}^{(2)}}{\partial x_1} + \frac{\partial M_{22}^{(2)}}{\partial x_2} - N_{23}^{(2)} - \frac{h_2N_{23}^{(c)}}{2h} =$$
$$-\frac{\rho_2h_2^3}{12}\ddot{\phi}_2^{(2)} - \rho_chh_2\left(\frac{\ddot{v}_0^{(2)}}{6} + \frac{\ddot{v}_0^{(1)}}{12} + \frac{h_2}{12}\ddot{\theta}_2^{(2)} - \frac{h_1}{24}\ddot{\theta}_2^{(1)}\right) \tag{28.h}$$

$$\frac{\partial N_{13}^{(1)}}{\partial x_1} + \frac{\partial N_{13}^{(2)}}{\partial x_1} + \frac{\partial N_{23}^{(1)}}{\partial x_2} + \frac{\partial N_{23}^{(2)}}{\partial x_2}$$
$$+ \frac{\partial N_{13}^{(c)}}{\partial x_1} + \frac{\partial N_{23}^{(c)}}{\partial x_2} = (\rho_1h_1 + \rho_2h_2 + \rho_ch_c)\ddot{w}_0 \tag{28.i}$$

where the forces N and moments M are as follows:

$$N_{11}^{(i)} = \int_{-h_i/2}^{h_i/2} \sigma_{11}^{(i)} dx_3^{(i)}, N_{22}^{(i)} = \int_{-h_i/2}^{h_i/2} \sigma_{22}^{(i)} dx_3^{(i)}, N_{12}^{(i)} = \int_{-h_i/2}^{h_i/2} \sigma_{12}^{(i)} dx_3^{(i)},$$

$$N_{13}^{(i)} = \int_{-h_i/2}^{h_i/2} \sigma_{13}^{(i)} dx_3^{(i)}, N_{23}^{(i)} = \int_{-h_i/2}^{h_i/2} \sigma_{23}^{(i)} dx_3^{(i)},$$

$$N_{13}^{(c)} = \int_{-h_i/2}^{h_i/2} \sigma_{13}^{(c)} dx_3^{(c)}, N_{23}^{(c)} = \int_{-h_i/2}^{h_i/2} \sigma_{23}^{(c)} dx_3^{(c)},$$

$$M_{11}^{(i)} = \int_{-h_i/2}^{h_i/2} x_3^{(i)} \sigma_{11}^{(i)} dx_3^{(i)}, M_{22}^{(i)} = \int_{-h_i/2}^{h_i/2} x_3^{(i)} \sigma_{22}^{(i)} dx_3^{(i)}, M_{12}^{(i)} = \int_{-h_i/2}^{h_i/2} x_3^{(i)} \sigma_{12}^{(i)} dx_3^{(i)}.$$

(29)

The essential boundary conditions at $x_1 = 0$, a are:

$$u_0^{(1)} = v_0^{(1)} = \theta_1^{(1)} = \theta_2^{(1)} = u_0^{(2)} = v_0^{(2)} = \theta_1^{(2)} = \theta_2^{(2)} = w_0 = 0 \quad (30)$$

The natural boundary conditions at $x_1 = 0$, a are:

$$N_{11}^{(1)} = N_{12}^{(1)} = M_{11}^{(1)} = M_{12}^{(1)} = N_{11}^{(2)} = N_{12}^{(2)} = M_{11}^{(2)}$$
$$= M_{12}^{(2)} = N_{13}^{(1)} + N_{13}^{(2)} + N_{13}^{(c)} = 0$$

(31)

The essential boundary conditions at $x_2 = 0$, b are:

$$u_0^{(1)} = v_0^{(1)} = \theta_1^{(1)} = \theta_2^{(1)} = u_0^{(2)} = v_0^{(2)} = \theta_1^{(2)} = \theta_2^{(2)} = w_0 = 0 \quad (32)$$

The natural boundary conditions at $x_2 = 0$, b are:

$$N_{12}^{(1)} = N_{22}^{(1)} = M_{12}^{(1)} = M_{22}^{(1)} = N_{12}^{(2)} = N_{22}^{(2)} = M_{12}^{(2)}$$
$$= M_{22}^{(2)} = N_{23}^{(1)} + N_{23}^{(2)} + N_{23}^{(c)} = 0$$

(33)

For the free vibration problem, the solutions with annular frequency ω were

$$u_0^{(i)} = \overline{u}_0^{(i)} e^{i\omega t}, v_0^{(i)} = \overline{v}_0^{(i)} e^{i\omega t}, \theta_1^{(i)} = \overline{\theta}_1^{(i)} e^{i\omega t}, \theta_2^{(i)} = \overline{\theta}_2^{(i)} e^{i\omega t}, w_0 = \overline{w}_0 e^{i\omega t} \quad (34)$$

3. Spectral collocation method

In this study, a spectral collocation method was utilized. The following non-dimensional variables were introduced:

$$\overline{\xi} = \frac{2x_1}{a} - 1, \overline{\eta} = \frac{2x_2}{b} - 1, U^{(i)} = \frac{\overline{u}_0^{(i)}}{h}, V^{(i)} = \frac{\overline{v}_0^{(i)}}{h}, \Theta_1^{(i)} = \overline{\theta}_1^{(i)}, \Theta_2^{(i)} = \overline{\theta}_2^{(i)}, W = \frac{\overline{w}_0}{h}$$

(35)

The displacement vector at the $(M + 1) \times (M + 1)$ collocation points is described as

$$W = \begin{bmatrix} U_{(1,1)}^{(1)} & U_{(1,2)}^{(1)} & \cdots & U_{(M+1,M+1)}^{(1)} & V_{(1,1)}^{(1)} & V_{(1,2)}^{(1)} & \cdots & V_{(M+1,M+1)}^{(1)} \\ \Theta_{1(1,1)}^{(1)} & \Theta_{1(1,2)}^{(1)} & \cdots & \Theta_{1(M+1,M+1)}^{(1)} & \Theta_{2(1,1)}^{(1)} & \Theta_{2(1,2)}^{(1)} & \cdots & \Theta_{2(M+1,M+1)}^{(1)} \\ & W_{(1,1)} & W_{(1,2)} & \cdots & W_{(M+1,M+1)} \\ U_{(1,1)}^{(2)} & U_{(1,2)}^{(2)} & \cdots & U_{(M+1,M+1)}^{(2)} & V_{(1,1)}^{(2)} & V_{(1,2)}^{(2)} & \cdots & V_{(M+1,M+1)}^{(2)} \\ \Theta_{1(1,1)}^{(2)} & \Theta_{1(1,2)}^{(2)} & \cdots & \Theta_{1(M+1,M+1)}^{(2)} & \Theta_{2(1,1)}^{(2)} & \Theta_{2(1,2)}^{(2)} & \cdots & \Theta_{2(M+1,M+1)}^{(2)} \end{bmatrix}^{\mathrm{T}}$$

(36)

where the superscript "T" means "transpose".

By substituting the non-dimensional variables in Eq. (35) and the harmonic solutions in Eq. (34) into Eqs. (28.a) through (28.i), the equations of motion using the spectral collocation method are

$$LW = \omega^2 RW \quad (37)$$

$$L = [L_1; \quad L_2; \quad \cdots \quad L_9] \quad (38)$$

$$R = [R_1; \quad R_2; \quad \cdots \quad R_9] \quad (39)$$

The left-hand sides of Eq. (37) are

$$L_1 = \frac{4E_1 h_1 h}{a^2(1 - \nu_1^2)}(E_1 \otimes D_2 \otimes E) + \frac{4E_1 h_1 h \nu_1}{ab(1 - \nu_1^2)}(E_2 \otimes D_1 \otimes D_1)$$
$$+ \frac{4G_1 h_1 h}{b^2}(E_1 \otimes E \otimes D_2) + \frac{4G_1 h_1 h}{ab}(E_2 \otimes D_1 \otimes D_1)$$
$$+ \frac{2G_c h}{a}(E_5 \otimes D_1 \otimes E) + G_c(E_6 \otimes E \otimes E)$$
$$- G_c(E_1 \otimes E \otimes E) + \frac{G_c h_2}{2h}(E_8 \otimes E \otimes E) + \frac{G_c h_1}{2h}(E_3 \otimes E \otimes E)$$

(40.a)

$$L_2 = \frac{4E_2 h_2 h}{a^2(1 - \nu_2^2)}(E_6 \otimes D_2 \otimes E) + \frac{4E_2 h_2 h \nu_2}{ab(1 - \nu_2^2)}(E_7 \otimes D_1 \otimes D_1)$$
$$+ \frac{4G_2 h_2 h}{b^2}(E_6 \otimes E \otimes D_2) + \frac{4G_2 h_2 h}{ab}(E_7 \otimes D_1 \otimes D_1)$$
$$- \frac{2G_c h}{a}(E_5 \otimes D_1 \otimes E) - G_c(E_6 \otimes E \otimes E)$$
$$+ G_c(E_1 \otimes E \otimes E) - \frac{G_c h_2}{2h}(E_8 \otimes E \otimes E) - \frac{G_c h_1}{2h}(E_3 \otimes E \otimes E)$$

(40.b)

$$L_3 = \frac{4G_1 h_1 h}{ab}(E_1 \otimes D_1 \otimes D_1) + \frac{4G_1 h_1 h}{a^2}(E_2 \otimes D_2 \otimes E)$$
$$+ \frac{4E_1 h_1 h}{b^2(1 - \nu_1^2)}(E_2 \otimes E \otimes D_2) + \frac{4E_1 h_1 h \nu_1}{ab(1 - \nu_1^2)}(E_1 \otimes D_1 \otimes D_1)$$
$$+ \frac{2G_c h}{b}(E_5 \otimes E \otimes D_1) + G_c(E_7 \otimes E \otimes E)$$
$$- G_c(E_2 \otimes E \otimes E) + \frac{G_c h_2}{2h}(E_9 \otimes E \otimes E) + \frac{G_c h_1}{2h}(E_4 \otimes E \otimes E)$$

(40.c)

$$L_4 = \frac{4G_2 h_2 h}{ab}(E_6 \otimes D_1 \otimes D_1) + \frac{4G_2 h_2 h}{a^2}(E_7 \otimes D_2 \otimes E)$$
$$+ \frac{4E_2 h_2 h}{b^2(1 - \nu_2^2)}(E_7 \otimes E \otimes D_2) + \frac{4E_2 h_2 h \nu_2}{ab(1 - \nu_2^2)}(E_6 \otimes D_1 \otimes D_1)$$
$$- \frac{2G_c h}{b}(E_5 \otimes E \otimes D_1) - G_c(E_7 \otimes E \otimes E)$$
$$+ G_c(E_2 \otimes E \otimes E) - \frac{G_c h_2}{2h}(E_9 \otimes E \otimes E) - \frac{G_c h_1}{2h}(E_4 \otimes E \otimes E)$$

(40.d)

$$L_5 = -\frac{E_1 h_1^3}{3a^2(1 - \nu_1^2)}(E_3 \otimes D_2 \otimes E) - \frac{E_1 h_1^3 \nu_1}{3ab(1 - \nu_1^2)}(E_4 \otimes D_1 \otimes D_1)$$
$$- \frac{G_1 h_1^3}{3b^2}(E_3 \otimes E \otimes D_2) - \frac{G_1 h_1^3}{3ab}(E_4 \otimes D_1 \otimes D_1) - \frac{2\kappa^2 G_1 h_1 h}{a}(E_5 \otimes D_1 \otimes E)$$
$$+ \kappa^2 G_1 h_1(E_3 \otimes E \otimes E) + \frac{G_c h_1}{a}(E_5 \otimes D_1 \otimes E) + \frac{G_c h_1}{2}(E_6 \otimes E \otimes E)$$
$$- \frac{G_c h_1}{2}(E_1 \otimes E \otimes E) + \frac{G_c h_1 h_2}{4h}(E_8 \otimes E \otimes E) + \frac{G_c h_1^2}{4h}(E_3 \otimes E \otimes E)$$

(40.e)

$$L_6 = -\frac{E_2 h_2^3}{3a^2(1 - \nu_2^2)}(E_8 \otimes D_2 \otimes E) - \frac{E_2 h_2^3 \nu_2}{3ab(1 - \nu_2^2)}(E_9 \otimes D_1 \otimes D_1)$$
$$- \frac{G_2 h_2^3}{3b^2}(E_8 \otimes E \otimes D_2) - \frac{G_2 h_2^3}{3ab}(E_9 \otimes D_1 \otimes D_1) - \frac{2\kappa^2 G_2 h_2 h}{a}(E_5 \otimes D_1 \otimes E)$$
$$+ \kappa^2 G_2 h_2(E_8 \otimes E \otimes E) + \frac{G_c h_2 h}{a}(E_5 \otimes D_1 \otimes E) + \frac{G_c h_2}{2}(E_6 \otimes E \otimes E)$$
$$- \frac{G_c h_2}{2}(E_1 \otimes E \otimes E) + \frac{G_c h_2^2}{4h}(E_8 \otimes E \otimes E) + \frac{G_c h_1 h_2}{4h}(E_3 \otimes E \otimes E)$$
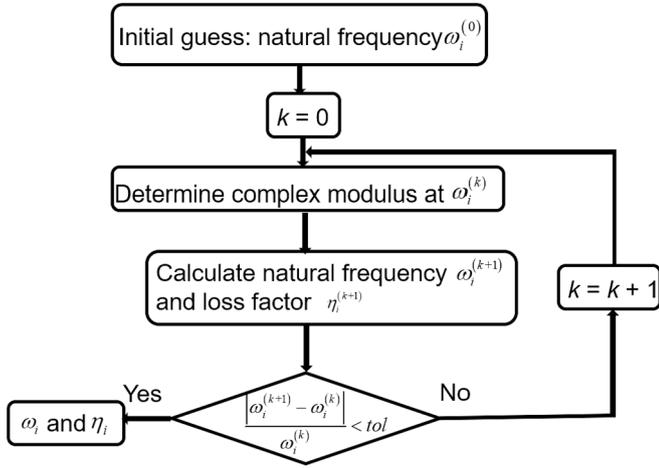
(40.f)

Fig. 3. Procedure to solve frequency-dependent eigenvalue problem.
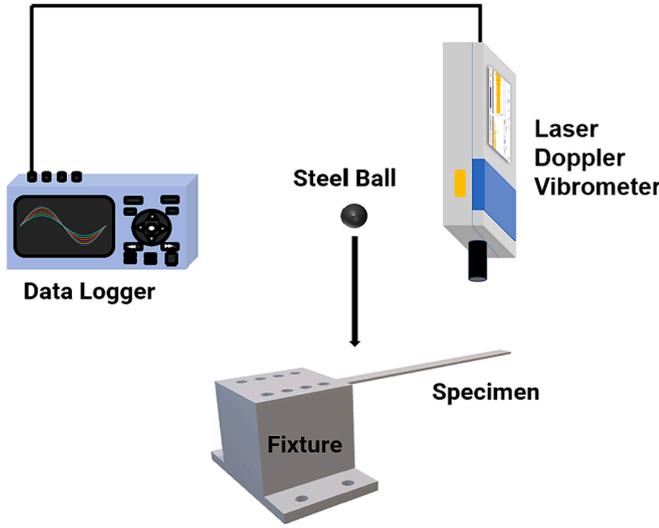

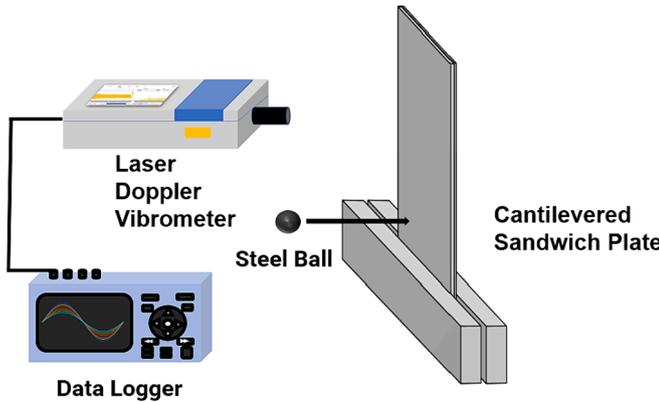Fig. 4. Schematic of experimental setup of a cantilevered beam.

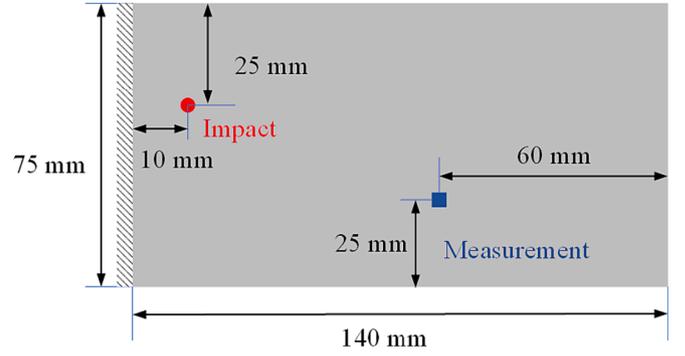Fig. 5. Schematic of experimental setup of a cantilevered sandwich plate.

Fig. 6. Impact and measurement locations of cantilevered sandwich plates.

$$L_7 = -\frac{G_1 h_1^3}{3ab}(E_3 \otimes D_1 \otimes D_1) - \frac{G_1 h_1^3}{3a^2}(E_4 \otimes D_2 \otimes E)$$
$$-\frac{E_1 h_1^3}{3b^2(1-\nu_1^2)}(E_4 \otimes E \otimes D_2) - \frac{E_1 h_1^3 \nu_1}{3ab(1-\nu_1^2)}(E_3 \otimes D_1 \otimes D_1)$$
$$-\frac{2\kappa^2 G_1 h_1 h}{b}(E_5 \otimes E \otimes D_1) + \kappa^2 G_1 h_1(E_4 \otimes E \otimes E)$$
$$+\frac{G_c h_1 h}{b}(E_5 \otimes E \otimes D_1) + \frac{G_c h_1}{2}(E_7 \otimes E \otimes E)$$
$$-\frac{G_c h_1}{2}(E_2 \otimes E \otimes E) + \frac{G_c h_1 h_2}{4h}(E_9 \otimes E \otimes E) + \frac{G_c h_1^2}{4h}(E_4 \otimes E \otimes E)$$
(40.g)

$$L_8 = -\frac{G_2 h_2^3}{3ab}(E_8 \otimes D_1 \otimes D_1) - \frac{G_2 h_2^3}{3a^2}(E_9 \otimes D_2 \otimes E)$$
$$-\frac{E_2 h_2^3}{3b^2(1-\nu_2^2)}(E_9 \otimes E \otimes D_2) - \frac{E_2 h_2^3 \nu_2}{3ab(1-\nu_2^2)}(E_8 \otimes D_1 \otimes D_1)$$
$$-\frac{2\kappa^2 G_2 h_2 h}{b}(E_5 \otimes E \otimes D_1) + \kappa^2 G_2 h_2(E_9 \otimes E \otimes E)$$
$$+\frac{G_c h_2 h}{b}(E_5 \otimes E \otimes D_1) + \frac{G_c h_2}{2}(E_7 \otimes E \otimes E)$$
$$-\frac{G_c h_2}{2}(E_2 \otimes E \otimes E) + \frac{G_c h_2^2}{4h}(E_9 \otimes E \otimes E) + \frac{G_c h_1 h_2}{4h}(E_4 \otimes E \otimes E)$$
(40.h)

$$L_9 = \left(\kappa^2 G_1 h_1 + \kappa^2 G_2 h_2 + G_c h\right)\left[\frac{4h}{a^2}(E_5 \otimes D_2 \otimes E) + \frac{4h}{b^2}(E_5 \otimes E \otimes D_2)\right]$$
$$-\frac{2\kappa^2 G_1 h_1}{a}(E_3 \otimes D_1 \otimes E) - \frac{2\kappa^2 G_1 h_1}{b}(E_4 \otimes E \otimes D_1) - \frac{2\kappa^2 G_2 h_2}{a}(E_8 \otimes D_1 \otimes E)$$
$$-\frac{2\kappa^2 G_2 h_2}{b}(E_9 \otimes E \otimes D_1) + \frac{G_c h_2}{a}(E_8 \otimes D_1 \otimes E) + \frac{G_c h_1}{a}(E_3 \otimes D_1 \otimes E)$$
$$+\frac{G_c h_2}{b}(E_9 \otimes E \otimes D_1) + \frac{G_c h_1}{b}(E_4 \otimes E \otimes D_1) + \frac{2G_c h}{a}(E_6 \otimes D_1 \otimes E)$$
$$-\frac{2G_c h}{a}(E_1 \otimes D_1 \otimes E) + \frac{2G_c h}{b}(E_7 \otimes E \otimes D_1) - \frac{2G_c h}{b}(E_2 \otimes E \otimes D_1)$$
(40.i)

The right-hand sides of Eq. (37) are

$$R_1 = -\rho_1 h_1 h(E_1 \otimes E \otimes E) - \rho_c h\left[\frac{h}{6}(E_6 \otimes E \otimes E) + \frac{h}{3}(E_1 \otimes E \otimes E)\right.$$
$$\left. + \frac{h_2}{12}(E_8 \otimes E \otimes E) - \frac{h_1}{6}(E_3 \otimes E \otimes E)\right]$$
(41.a)

$$R_2 = -\rho_2 h_2 h(E_6 \otimes E \otimes E) - \rho_c h\left[\frac{h}{3}(E_6 \otimes E \otimes E) + \frac{h}{6}(E_1 \otimes E \otimes E)\right.$$
$$\left. + \frac{h_2}{6}(E_8 \otimes E \otimes E) - \frac{h_1}{12}(E_3 \otimes E \otimes E)\right]$$
(41.b)

Table 1

Convergence study of first eight modes with the number of CGL points N.

N	Mode	1	2	3	4	5	6	7	8
10	Frequency (Hz)	39.7	66.9	89.2	110.8	113.8	155.2	163.9	171.5
	Loss factor	0.117	0.133	0.157	0.163	0.167	0.181	0.189	0.187
14	Frequency (Hz)	39.7	67.0	89.3	110.9	113.9	155.3	164.0	170.3
	Loss factor	0.117	0.134	0.157	0.163	0.168	0.181	0.190	0.183
18	Frequency (Hz)	39.7	67.0	89.3	110.9	113.9	155.4	164.0	170.3
	Loss factor	0.117	0.134	0.158	0.163	0.168	0.181	0.190	0.183
22	Frequency (Hz)	39.7	67.0	89.3	110.9	113.9	155.4	164.0	170.3
	Loss factor	0.117	0.134	0.158	0.163	0.168	0.181	0.190	0.183
26	Frequency (Hz)	39.7	67.0	89.3	110.9	113.9	155.4	164.0	170.3
	Loss factor	0.117	0.134	0.158	0.163	0.168	0.181	0.190	0.183

Table 2

Comparison with published results for the 0.8 mm-0.0508 mm-0.8 mm thick sandwich plate.

Mode	Experiment [16]		GAMA [16]		Present study	
	Frequency (Hz)	Loss factor	Frequency (Hz)	Loss factor	Frequency (Hz)	Loss factor
1	38.0	0.092	39.5	0.122	39.7	0.117
2	68.5	–	67.6	–	67.0	0.134
3	90.3	0.158	90.3	0.166	89.3	0.158
4	109.1	0.186	112.6	0.183	110.9	0.163
5	120.0	–	115.6	–	113.9	0.168
6	–	–	159.9	–	155.4	0.181
7	162.0	–	167.1	–	164.0	0.190
8	187.0	–	174.3	–	170.3	0.183

Table 3

Comparison with published results for the 0.4 mm-0.0508 mm-0.8 mm thick sandwich plate.

Mode	Experiment [16]		GAMA [16]		Present study	
	Frequency (Hz)	Loss factor	Frequency (Hz)	Loss factor	Frequency (Hz)	Loss factor
1	29.8	0.062	30.6	0.0911	30.8	0.086
2	51.8	–	52.7	–	52.3	0.095
3	71.7	0.116	70.5	0.117	70.0	0.111
4	85.0	0.139	87.5	0.131	86.8	0.116
5	89.8	–	90.3	–	89.3	0.120
6	125.2	–	124.7	–	121.8	0.133
7	131.0	–	130.0	–	128.8	0.140
8	152.0	–	136.0	–	133.5	0.136
9	169.0	–	151.0	–	147.2	0.144
10	178.0	–	171.3	–	167.0	0.144

Table 4

Comparison with published results for the 0.4 mm-0.127 mm-0.8 mm thick sandwich plate.

Mode	Experiment [16]		GAMA [16]		Present study	
	Frequency (Hz)	Loss factor	Frequency (Hz)	Loss factor	Frequency (Hz)	Loss factor
1	27.0	0.114	30.2	0.177	30.4	0.168
2	51.0	–	51.5	–	50.9	0.178
3	72.0	0.207	67.9	0.211	67.1	0.199
4	82.0	0.173	83.6	0.232	83.1	0.206
5	88.0	–	86.5	–	85.2	0.210
6	117.0	–	117.8	–	115.2	0.229
7	126.0	–	121.8	–	121.0	0.239
8	139.0	–	128.3	–	125.9	0.237
9	–	–	141.1	–	138.1	0.244
10	168.0	–	160.7	–	156.7	0.247

$$R_3 = -\rho_1 h_1 h(E_2 \otimes E \otimes E) - \rho_c h \left[\frac{h}{6}(E_7 \otimes E \otimes E) + \frac{h}{3}(E_2 \otimes E \otimes E) \right.$$
$$\left. + \frac{h_2}{12}(E_9 \otimes E \otimes E) - \frac{h_1}{6}(E_4 \otimes E \otimes E) \right]$$
(41.c)

$$R_4 = -\rho_2 h_2 h(E_7 \otimes E \otimes E) - \rho_c h \left[\frac{h}{3}(E_7 \otimes E \otimes E) + \frac{h}{6}(E_2 \otimes E \otimes E) \right.$$
$$\left. + \frac{h_2}{6}(E_9 \otimes E \otimes E) - \frac{h_1}{12}(E_4 \otimes E \otimes E) \right]$$
(41.d)

$$R_5 = -\frac{\rho_1 h_1^3}{12}(E_3 \otimes E \otimes E) - \rho_c h h \left[\frac{h}{12}(E_6 \otimes E \otimes E) + \frac{h}{6}(E_1 \otimes E \otimes E) \right.$$
$$\left. + \frac{h_2}{24}(E_8 \otimes E \otimes E) - \frac{h_1}{12}(E_3 \otimes E \otimes E) \right]$$
(41.e)

$$R_6 = -\frac{\rho_2 h_2^3}{12}(E_8 \otimes E \otimes E) - \rho_c h h_2 \left[\frac{h}{6}(E_6 \otimes E \otimes E) + \frac{h}{12}(E_1 \otimes E \otimes E) \right.$$
$$\left. + \frac{h_2}{12}(E_8 \otimes E \otimes E) - \frac{h_1}{24}(E_3 \otimes E \otimes E) \right]$$
(41.f)

$$R_7 = \frac{\rho_1 h_1^3}{12}(E_4 \otimes E \otimes E) - \rho_c h h_1 \left[\frac{h}{12}(E_7 \otimes E \otimes E) + \frac{h}{6}(E_2 \otimes E \otimes E) \right.$$
$$\left. + \frac{h_2}{24}(E_9 \otimes E \otimes E) - \frac{h_1}{12}(E_4 \otimes E \otimes E) \right]$$
(41.g)

$$R_8 = \frac{\rho_2 h_2^3}{12}(E_9 \otimes E \otimes E) - \rho_c h h_2 \left[\frac{h}{6}(E_7 \otimes E \otimes E) + \frac{h}{12}(E_2 \otimes E \otimes E) \right.$$
$$\left. + \frac{h_2}{12}(E_9 \otimes E \otimes E) - \frac{h_1}{24}(E_4 \otimes E \otimes E) \right]$$
(41.h)

$$R_9 = -(\rho_1 h_1 + \rho_2 h_2 + \rho_c h)h(E_5 \otimes E \otimes E)$$
(41.i)

where E_j is the jth row unit vector with nine elements; E is an identity matrix of size $M + 1$; D_1 is a Chebyshev differentiation matrix [39]; $D_2 = (D_1)^2$ is a second-order differentiation matrix; and $\otimes$ is the Kronecker product.

W_B and W_I are boundary Chebysheve–Gauss–Lobatto (CGL) points and interior CGL points, respectively.

$$W_B = Z_B W, \quad W_I = Z_I W$$
(42)

$$Z_B = \begin{bmatrix} e_1 & \cdots & e_{M+1} & \cdots & e_{M(M+1)+1} & \cdots & e_{(M+1)^2} & \cdots & e_{9(M+1)^2} \end{bmatrix}^T$$
(43)

$$Z_I = \begin{bmatrix} e_{M+3} & \cdots & e_{2M+1} & e_{2M+4} & \cdots & e_{3M+2} & \cdots \end{bmatrix}^T$$
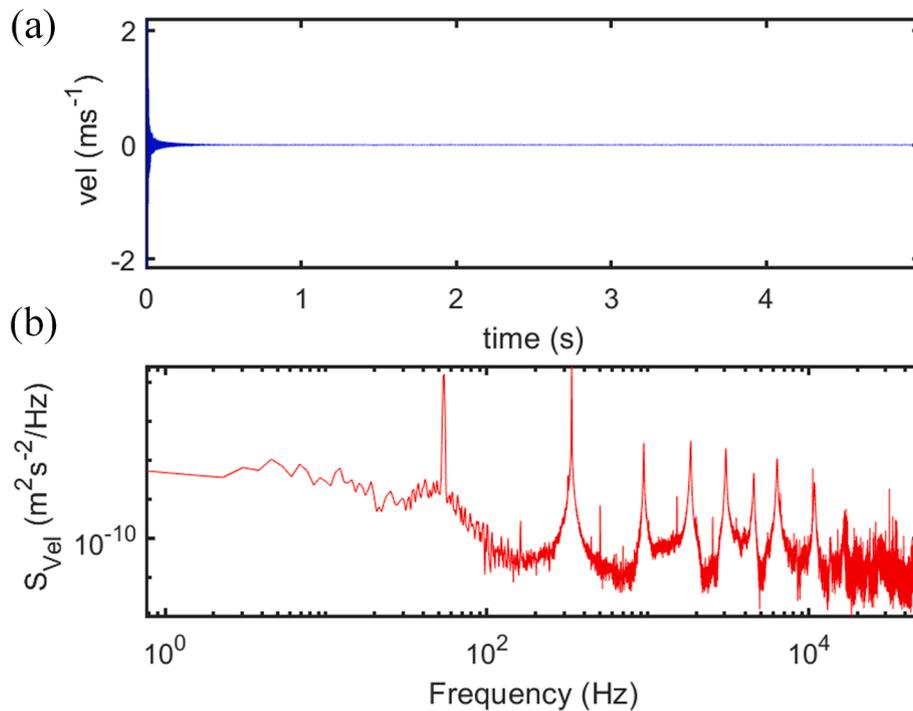(44)

Fig. 7. Velocity history (a) and FFT results (b) of a two-layer beam with length 150 mm.

where e_j denotes the jth unit vector with $(M+1)^2$ elements. Further details can be found in [45] and [46].

The boundary conditions are written as

$$B_B W_B + B_I W_I = 0 \tag{45}$$

$$B_B = B Z_B^T, B_I = B Z_I^T \tag{46}$$

where B denotes the boundary conditions of four edges with size $36M \times 9(M+1)^2$.

The standard eigenvalue equation can be obtained using Eqs. (37) and (45) as

$$\left(Z_I L Z_I^T - Z_I L Z_B^T B_B^{-1} B_I\right) W_I = \omega^2 Z_I R Z_I^T W_I \tag{47}$$

The boundary conditions for CCCC and CFFF are listed in **Appendix A and B**, respectively. The procedure illustrated in Fig. 3 was employed to deal with the frequency-dependent complex eigenvalue problem in Eq. (47).

4. Experimental setup

The frequency-dependent viscoelastic materials were obtained using the Oberst beam method [38]. Two-part liquid epoxy adhesives (DENATITE 2204, Nagase Chemtex Corp., Osaka, Japan) and an aluminum beam were used to create a two-layer specimen. The adhesive was cured at 100 ℃ for 30 mins. The length, width, and thickness of the aluminum beam were 200, 10, and 1.50 mm, respectively. The thickness of the adhesive on the aluminum beam was 0.77 mm. The specimen was fixed to the fixture, as Fig. 4 shows. A steel ball was used to strike the specimen and excite it at high frequencies. The impact point was located 20 mm from the fixed edge. Three experiments were conducted with different lengths (150, 130, and 110 mm). A laser Doppler vibrometer (VibroGo, Polytec) was used to record velocity histories. The sampling frequency 100 kHz and the sampling time 4 s were used. The distances between the measurement location and free edge in the three experiments were 85, 60, and 60 mm. All the experiments were conducted at 20 ℃.

Three sandwich plates were fabricated with different viscoelastic cores. The constraining plates and base plates' thicknesses are 0.483 and 0.779 mm, respectively. The length and width of the specimens were 140 and 75 mm, respectively. The viscoelastic core of Specimen 1 was DENATITE 2204, and was 0.199 mm thick. The viscoelastic core of Specimen 2 was 3 M polymer 242NR01, and was 0.0254 mm thick. The viscoelastic core of Specimen 3 was 3 M polymer 242NR02, and was 0.0508 mm thick. The experimental setup for measuring dynamic properties of a cantilevered sandwich plate is illustrated in Fig. 5. The measurement and impact locations are shown in Fig. 6.

5. Results and discussion

5.1. Validation of present method

To validate the developed method, the theoretical data were compared with the data in [16]. The sandwich plates were 673.1 mm long, and 520.7 mm wide. The four edges were clamped. The constraining and base plates were made of aluminum. The Young's modulus 68.9 GPa, Poisson's ratio 0.3, and density 2740 kg/m³ were employed. 3 M Scotch damp ISD-112 was used to make specimens. The density of the core was 999 kg/m³. In their study, GAMA was exploited to solve the natural frequencies and loss factors of specimens. The GHM method was utilized to take the frequency-dependent complex properties into consideration.

$$G^* = G_0 \left[1 + \sum_{k}^{M} \tilde{\alpha}_k \frac{s^2 + 2\tilde{\zeta}_k \tilde{\omega}_k s}{s^2 + 2\tilde{\zeta}_k \tilde{\omega}_k s + \tilde{\omega}_k^2} \right] \tag{48}$$

where G^* and s are the complex shear modulus and operator in Laplace domain; G_0 is the equilibrium modulus. The parameters of three mini-oscillators at 20 ℃ are

$$\begin{bmatrix} \tilde{\alpha}_1 & \tilde{\alpha}_2 & \tilde{\alpha}_3 \end{bmatrix} = \begin{bmatrix} 1.557 & 6.39 & 32.8 \end{bmatrix} \tag{49}$$

$$\begin{bmatrix} \tilde{\omega}_1 & \tilde{\omega}_2 & \tilde{\omega}_3 \end{bmatrix} = \begin{bmatrix} 9993.3 & 20000 & 5e3 \end{bmatrix} \tag{50}$$
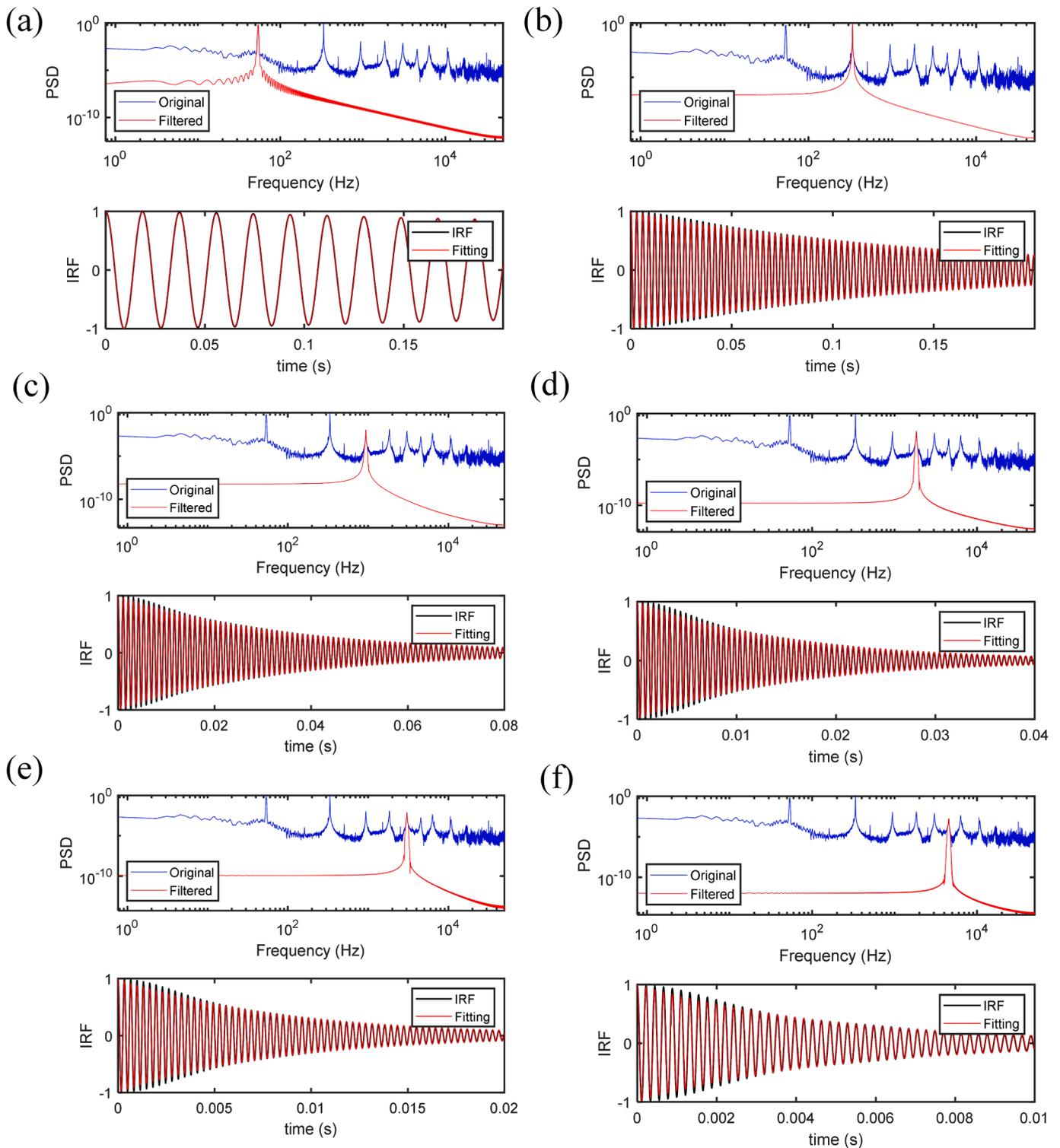
Fig. 8. Original and filtered PSD, and original and fitting IRF of the first six modes (a) Mode 1 (b) Mode 2 (c) Mode 3 (d) Mode 4 (e) Mode 5 (f) Mode 6.

$$\begin{bmatrix} \widetilde{\zeta}_1 & \widetilde{\zeta}_2 & \widetilde{\zeta}_3 \end{bmatrix} = \begin{bmatrix} 357.6 & 59.0 & 1.03 \end{bmatrix} \tag{51}$$

$$G_0 = 1.0e5 \tag{52}$$

A convergence study of the results of the first eight modes with the number of CGL points for a 0.8–0.0508–0.8 mm thick plate is provided in Table. 1. This proves that the spectral collocation method in solving free vibration problem of a sandwich plate exhibits high convergence rate. In the latter examples, 20 CGL points were used in each direction. Table. 2 shows a comparison of the present method with experimental and theoretical results of GAMA for the 0.8–0.0508–0.8 mm thick plate. The results from the GAMA and experimental measurements correlate well with the proposed method. Table. 3 shows a comparison of the present method with experimental and theoretical results of GAMA for the 0.4–0.0508–0.8 mm thick plate. As the thickness of the constraining plate decreased, the natural frequencies decreased. Table. 4 shows a comparative analysis of the proposed method with the experimental and
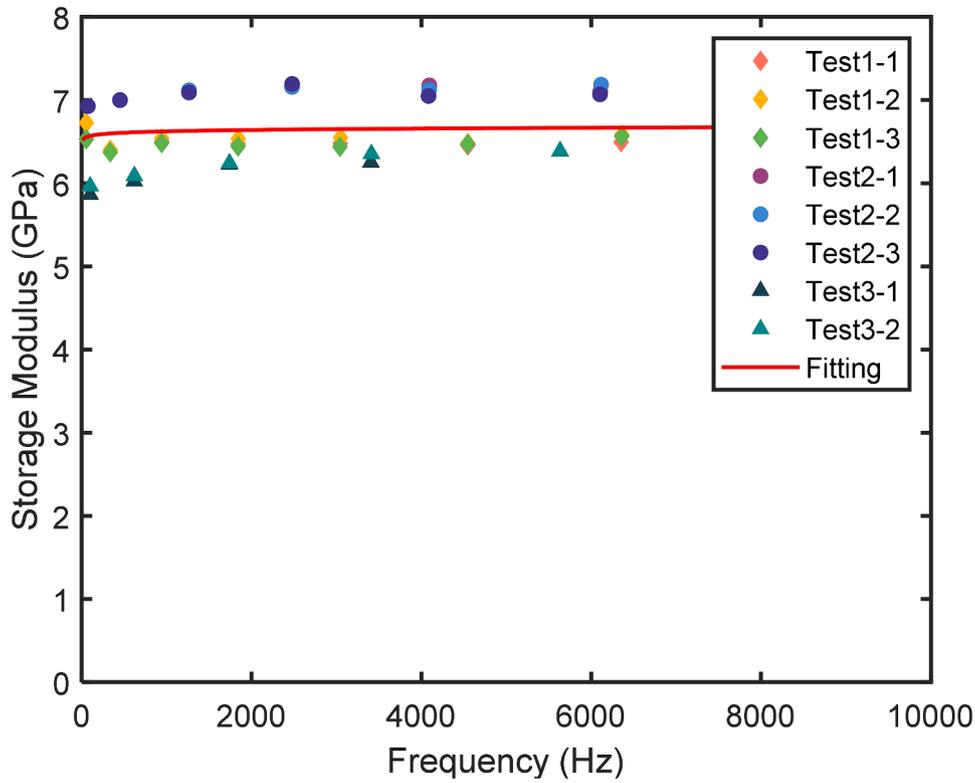
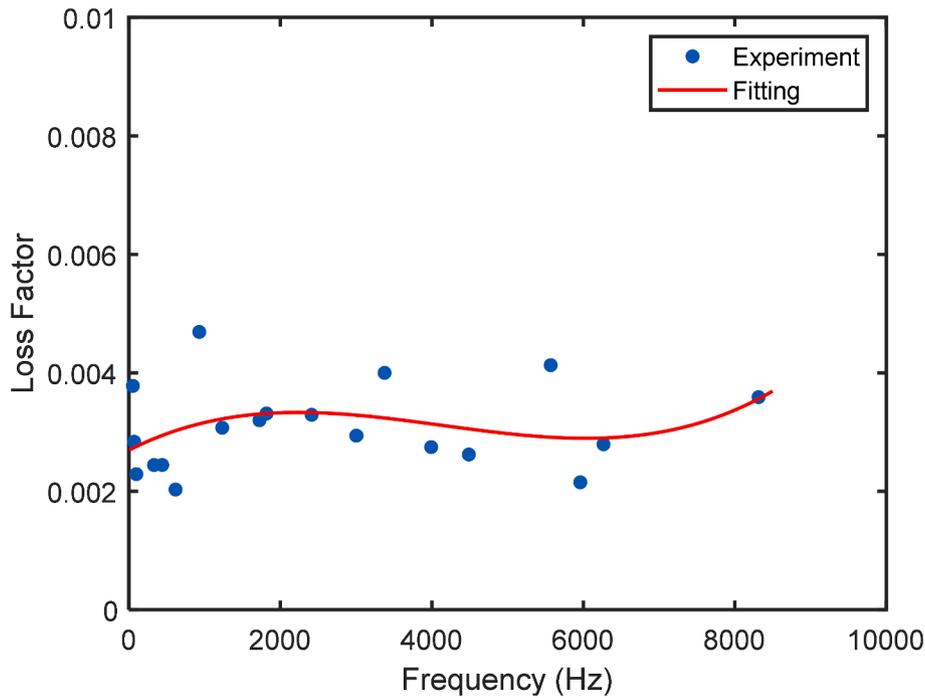**Fig. 9.** Variation in storage modulus with frequency.

Fig. 10. Variation in loss factor of aluminum beam with frequency.

theoretical data of GAMA for the 0.4–0.127–0.8 mm thick plate. As the thickness of the viscoelastic core increased, the natural frequencies decreased slightly and loss factors increased. In generally, the proposed method matches well with the GAMA results and experimental measurements for fully clamped rectangular sandwich plates in terms of loss factors and natural frequencies.

5.2. Viscoelastic properties of adhesive

To identify the specimens' loss factors and natural frequencies, a fast Fourier transform (FFT) was carried out on the measured velocity history. Based on the FFT results, the local peaks were chosen as the natural frequencies. Subsequently, a band-pass filter was applied to each natural frequency to get the modal response in time domain. The
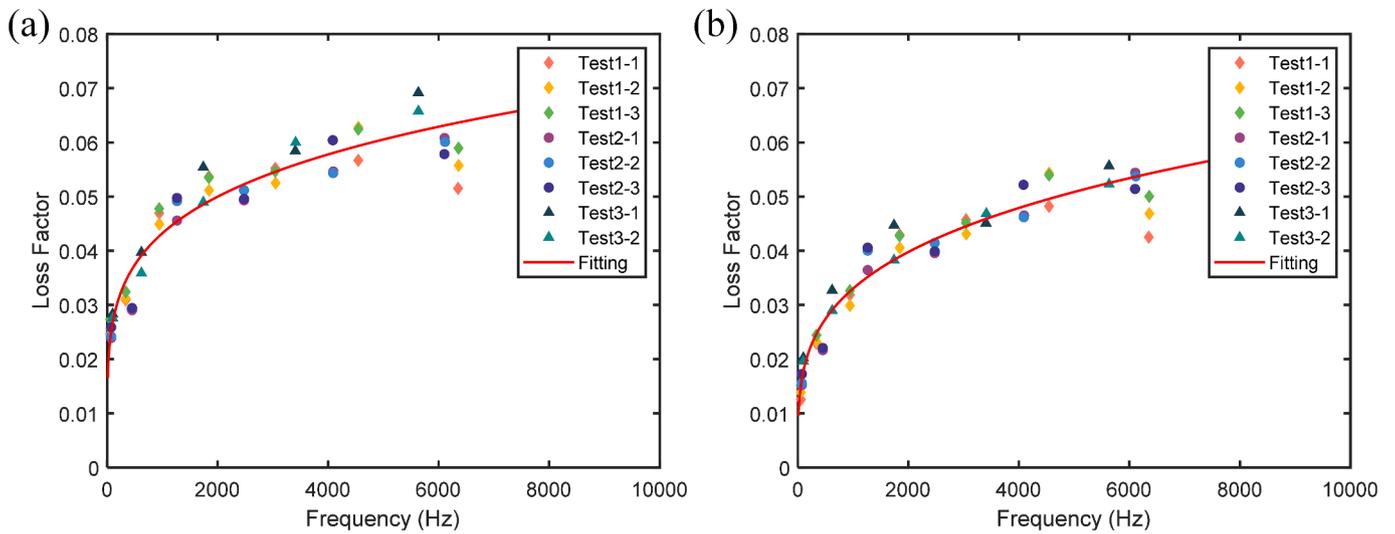
Fig. 11. Variation in loss factor of adhesive with frequency: (a) without base beam damping effect (b) with base beam damping effect.
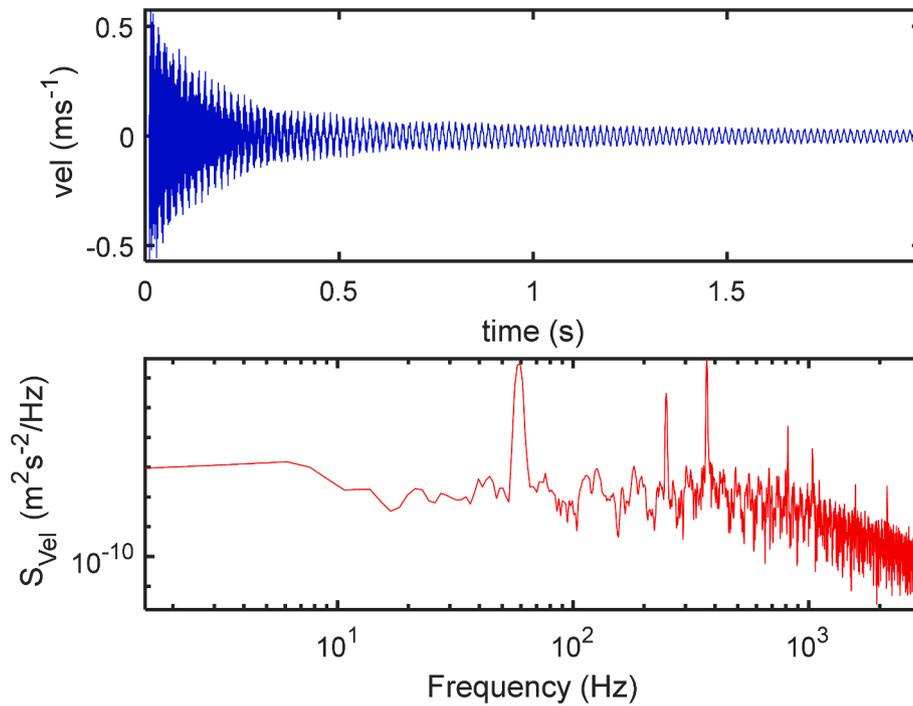

Fig. 12. (a) Velocity history (b) and FFT results for Specimen 1.

Table 5
Comparison between theoretical and experimental results for Specimen 1.

Mode	Theory		Experiment	
	Frequency (Hz)	Loss factor	Frequency (Hz)	Loss factor
1	64.1	0.0027	58.7	0.0038
2	254.0	0.0030	248.7	0.0015
3	396.5	0.0030	369.3	0.0047
4	832.7	0.0035	816.0	0.0034
5	1109.3	0.0034	1036.8	0.0078
6	1518.4	0.0035	–	–
7	1623.7	0.0037	1575.5	0.0048
8	2061.2	0.0038	–	–
9	2223.5	0.0038	2147.7	0.0039
10	2502.0	0.0033	–	–

autocorrelation function of the modal response was computed to obtain the IRF [51]. The damping factor of the corresponding mode was estimated by fitting an exponential decay function to the IRF. The measured velocity history and FFT result for a two-layer beam of 150 mm under impact loading are displayed in Fig. 7. Fig. 8 shows the original and filtered power spectral density (PSD) functions and the original and fitted IRFs of the first six modes. The damping ratio ξ is obtained from the fitted IRF. The relationship [52,53] between damping ratio ξ and the loss factor η is

$$\eta = 2\xi\sqrt{1 - \xi^2} \tag{53}$$

According to the Oberst beam method [38], the storage modulus can be obtained as
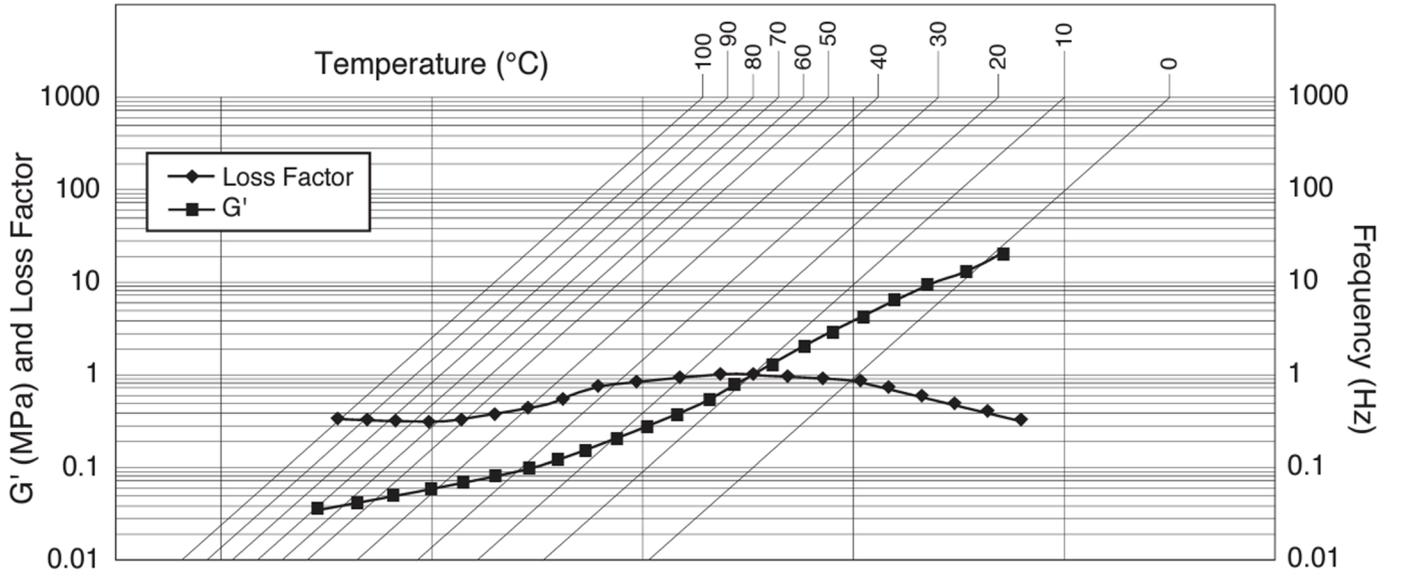
Fig. 13. 3M 242 ultra-pure viscoelastic damping polymer damping properties [55].
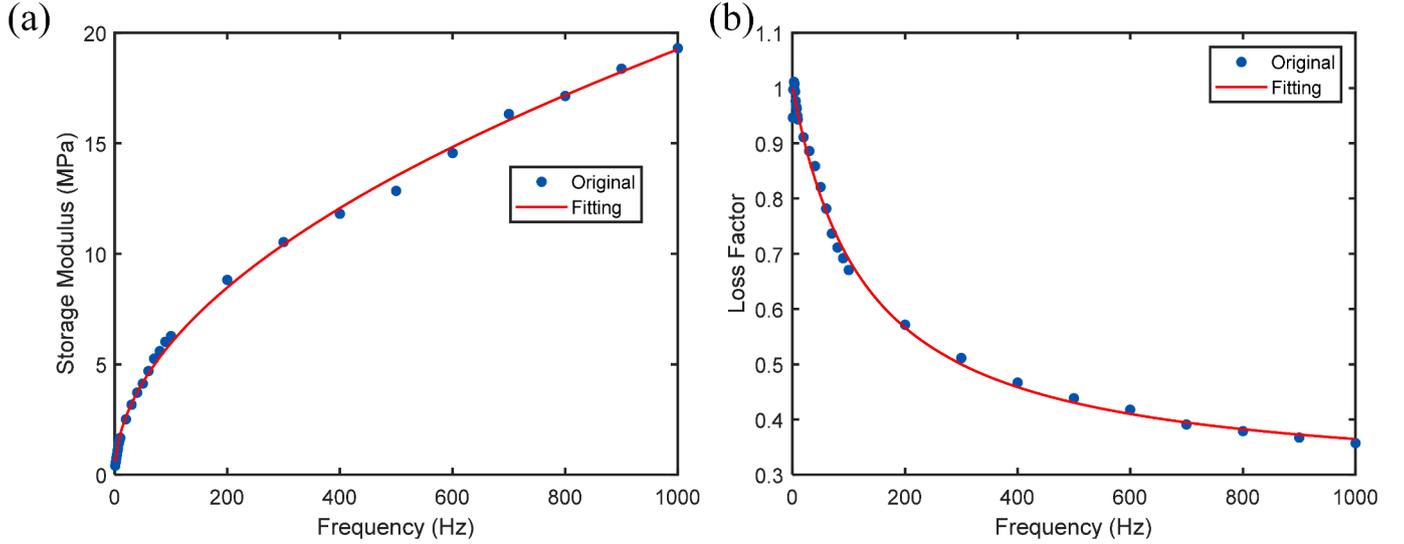

Fig. 14. (a) Storage modulus (b) Loss factor of 3M 242 polymer at 20 ℃.

$$E_a = \frac{E_b}{2H^3}\left[\alpha - \beta + \sqrt{(\alpha - \beta)^2 H^2 - 4H^2(1 - \alpha)}\right] \tag{54}$$

$$\alpha = (1 + DH)\left(\frac{f_j}{f_{0j}}\right)^2 \tag{55}$$

$$\beta = 4 + 6H + 4H^2 \tag{56}$$

$$e = \frac{\alpha - \beta + \sqrt{(\alpha - \beta)^2 H^2 - 4H^2(1 - \alpha)}}{2H^3} \tag{57}$$

where E_a and E_b are Young's moduli of the adhesive and the base beam, respectively; $D = \rho_a/\rho_b$; $H = h_a/h_b$; f_j and f_{0j} are the jth natural frequencies of the composite and base beam, respectively; ρ_a is the density of the adhesive; ρ_b is the density of the base beam; h_a and h_b are the thicknesses of adhesive and base beam, respectively.

The loss factor can be obtained by

$$\eta_a = \eta_{eff}\frac{1 + eH}{eH}\frac{1 + 4eH + 6eH^2 + 4eH^3 + e^2H^4}{3 + 6H + 4H^2 + 2eH^3 + e^2H^4} \tag{58}$$

where η_a and η_{eff} are the loss factors of the adhesive and the composite beam, respectively.

The low loss factor of an adhesive should be modified as

$$\eta_a = \left(\eta_{eff} - \eta_b\right)\frac{1 + eH}{eH}\frac{1 + 4eH + 6eH^2 + 4eH^3 + e^2H^4}{3 + 6H + 4H^2 + 2eH^3 + e^2H^4} + \eta_b \tag{59}$$

where η_b is the base beam's loss factor.

In the experiments, the Young's modulus 69 GPa and density 2711 kg/m³ were used for the base beam. The density of the adhesive was 1551 kg/m³. The Poisson's ratios of aluminum and DENATITE 2204 are 0.33 and 0.392, respectively. Fig. 9 shows the variation in the storage modulus of DENATITE 2204 with frequency. Test1, 2, and 3 are the impact tests of the two-layer beams with lengths of 150, 130, and 110 mm, respectively. Test1-1 was the first impact test of the 150 mm two-layer beam. The storage modulus can be fitted using the following sigmoidal function [54]:
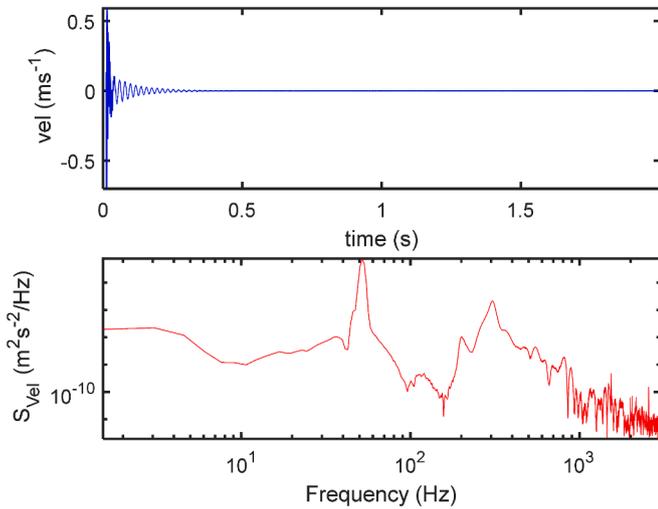
Fig. 15. (a) Velocity history (b) and FFT results for Specimen 2.

Table 6

Comparison between theoretical and experimental results for Specimen 2.

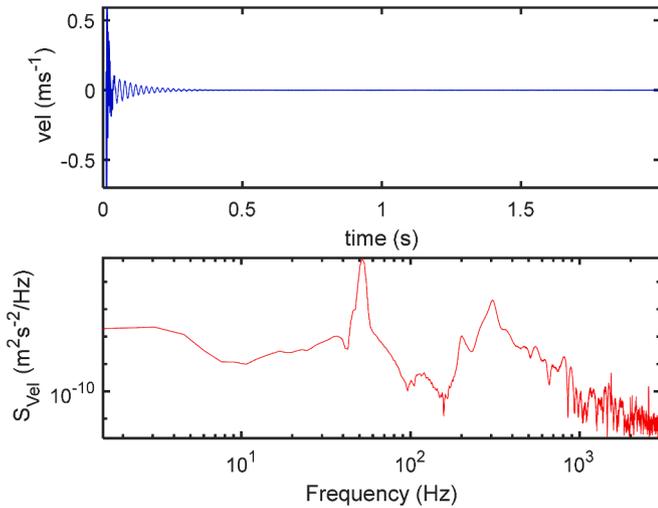| Mode	Theory		Experiment	
	Frequency (Hz)	Loss factor	Frequency (Hz)	Loss factor
1	54.7	0.0125	52.3	0.0201
2	207.0	0.0358	203.7	0.0273
3	334.1	0.0207	305.6	0.0261
4	685.8	0.0268	–	–
5	923.2	0.0233	–	–
6	1283.1	0.0149	–	–
7	1332.2	0.0276	–	–
8	1705.0	0.0238	–	–
9	1832.8	0.0268	–	–
10	2213.4	0.0297	–	–

Fig. 16. (a) Velocity history (b) and FFT results for Specimen 3.

$$E_a = -13.66\tanh(-0.0095\log(\omega) + 1.031) + 17 \quad [\text{GPa}] \tag{60}$$

The variation in aluminum's loss factor with frequency is illustrated in Fig. 10. The loss factor is fitted as follows:

$$\eta_b = 1.603\text{e} - 14f^3 - 1.989\text{e} - 10f^2 + 6.499\text{e} - 7f + 0.002694 \tag{61}$$

The variation in the adhesive's loss factor with frequency is shown in

Table 7

Comparison between theoretical and experimental results for Specimen 3.

Mode	Theory		Experiment	
	Frequency (Hz)	Loss factor	Frequency (Hz)	Loss factor
1	55.3	0.0212	52.3	0.0234
2	203.2	0.0556	209.4	0.0571
3	331.8	0.0376	320.4	0.0465
4	673.7	0.0431	–	–
5	907.5	0.0412	–	–
6	1278.8	0.0266	–	–
7	1299.8	0.0453	–	–
8	1672.3	0.0395	–	–
9	1783.9	0.0460	–	–
10	2143.1	0.0492	–	–

Fig. 11. The loss factors obtained using Eq. (58) and shown in Fig. 11 (a) is fitted as

$$\eta_a = 0.00694e^{0.2092\ln(\omega)} \tag{62}$$

The loss factors obtained using Eq. (59) and shown in Fig. 11 (b) is fitted as

$$\eta_a = 0.003164e^{0.2682\ln(\omega)} \tag{63}$$

Based on these results, it is essential to take the base beam's loss factor into account when measuring the loss factor of DENATITE 2204.

5.3. Comparison with experimental results

Fig. 12 (a) shows the measured velocity history of Specimen 1. Fig. 12 (b) shows the FFT results. Because the loss factor of DENATITE 2204 and thickness of the adhesive on the specimen were low, the effect of the aluminum plate's loss factor could not be ignored. In the calculation, the loss factor of aluminum in Eq. (59) was included. A comparison of theoretical and experimental results of Specimen 1 is listed in Table. 5. The results show that the impact of the aluminum plate's loss factor cannot be ignored. Fig. 13 shows the damping properties of 242 ultra-pure viscoelastic damping polymers [55]. The complex modulus at the desired frequency can be decided by drawing out a horizontal line from the target frequency until it bisects the intended target temperature isotherm. A vertical line is then extended from the cross point until it intersects the master curves. The loss factor and storage modulus are obtained from the left-hand scale of the interaction points. Fig. 14 shows complex modulus with frequency at 20 ℃. The storage modulus $G^{'}$ at 20 ℃ can be fitted as

$$G^{'} = 0.5687f^{0.5098} \quad [\text{MPa}] \tag{64}$$

The loss factor η_a at 20 ℃ can be fitted as:

$$\eta_a = \frac{0.2815f + 130.2}{f + 129.4} \tag{65}$$

The density of the adhesive was about 1000 kg/m^3. Fig. 15 (a) shows the measured velocity history of Specimen 2. Fig. 15 (b) shows the FFT results. The loss factor of 3 M 242 was significantly higher than that of DENATITE 2204. The velocity was damped rapidly. As shown in Fig. 15 (b), only three low modes were excited. Table. 6 shows a comparison with theoretical and experimental results of Specimen 2. Fig. 16 (a) shows the measured velocity history of Specimen 3. The FFT results are presented in Fig. 16 (b). Table. 7 shows a comparison of theoretical and experimental results of Specimen 3. Because the thickness of the adhesive on Specimen 3 was double that of the adhesive on Specimen 2, the loss factors of Specimen 3 were much higher than those of Specimen 2. The results indicated that the proposed method matched the experimental measurements well.

6. Conclusions

In this study, a spectral collocation method using a layer-wise plate theory was established to inspect vibration characteristics of sandwich plates with viscoelastic cores. Hamilton's principle was applied to get the equations of motion. To address the complex eigenvalue problem, an iterative algorithm was utilized. The proposed method was validated using published theoretical and experimental results for fully clamped rectangular sandwich plates. The modified Oberst beam method was applied by fitting the IRF to obtain the adhesive's frequency-dependent storage modulus and loss factor. The natural frequencies and corresponding loss factors of three sandwich plates with different adhesives were measured by conducting impact tests. For adhesives with low loss factors, the loss factors of the constraining and base plates must be considered. The numerical results from the present theoretical method agreed well with the measured results.

CRediT authorship contribution statement

Ming Ji: Conceptualization, Data curation, Investigation, Methodology, Software, Validation, Visualization, Writing – original draft, Writing – review & editing. **Chao Kang:** Data curation, Software, Writing – review & editing. **Yu Sekiguchi:** Conceptualization, Investigation, Writing – review & editing. **Masanobu Naito:** Funding acquisition, Project administration, Writing – review & editing. **Chiaki Sato:** Conceptualization, Funding acquisition, Project administration, Supervision, Writing – review & editing.

Declaration of competing interest

The authors declare that they have no known competing financial interests or personal relationships that could have appeared to influence the work reported in this paper.

Data availability

Data will be made available on request.

Acknowledgements

Appendix A. . Boundary conditions for CCCC

At $x_1 = 0$

$$\begin{aligned}(E_1 \otimes E_L)W &= (E_2 \otimes E_L)W = (E_3 \otimes E_L)W \\ &= (E_4 \otimes E_L)W = (E_5 \otimes E_L)W = (E_6 \otimes E_L)W \\ &= (E_7 \otimes E_L)W = (E_8 \otimes E_L)W = (E_9 \otimes E_L)W = 0\end{aligned} \tag{A.1}$$

At $x_1 = a$

$$\begin{aligned}(E_1 \otimes E_R)W &= (E_2 \otimes E_R)W = (E_3 \otimes E_R)W \\ &= (E_4 \otimes E_R)W = (E_5 \otimes E_R)W = (E_6 \otimes E_R)W \\ &= (E_7 \otimes E_R)W = (E_8 \otimes E_R)W = (E_9 \otimes E_R)W = 0\end{aligned} \tag{A.2}$$

At $x_2 = 0$

$$\begin{aligned}(E_1 \otimes E_B)W &= (E_2 \otimes E_B)W = (E_3 \otimes E_B)W \\ &= (E_4 \otimes E_B)W = (E_5 \otimes E_B)W = (E_6 \otimes E_B)W \\ &= (E_7 \otimes E_B)W = (E_8 \otimes E_B)W = (E_9 \otimes E_B)W = 0\end{aligned} \tag{A.3}$$

At $x_2 = b$

$$\begin{aligned}(E_1 \otimes E_T)W &= (E_2 \otimes E_T)W = (E_3 \otimes E_T)W \\ &= (E_4 \otimes E_T)W = (E_5 \otimes E_T)W = (E_6 \otimes E_T)W \\ &= (E_7 \otimes E_T)W = (E_8 \otimes E_T)W = (E_9 \otimes E_T)W = 0\end{aligned} \tag{A.4}$$

where $E_L = E(M+1,:) \otimes E$; $E_R = E(1,:) \otimes E$; $E_B = E \otimes E(M+1,:)$; $E_T = E \otimes E(1,:)$.

Appendix B. . Boundary conditions for CFFF

At $x_1 = 0$

$$\begin{aligned}(E_1 \otimes E_L)W &= (E_2 \otimes E_L)W = (E_3 \otimes E_L)W \\ &= (E_4 \otimes E_L)W = (E_5 \otimes E_L)W = (E_6 \otimes E_L)W \\ &= (E_7 \otimes E_L)W = (E_8 \otimes E_L)W = (E_9 \otimes E_L)W = 0\end{aligned} \tag{B.1}$$

At $x_1 = a$

$$\frac{1}{a}(E_1 \otimes D_R)W + \frac{\nu_1}{b}(E_2 \otimes E_{DR})W = \frac{1}{a}(E_6 \otimes D_R)W + \frac{\nu_1}{b}(E_7 \otimes E_{DR})W$$

$$= \frac{1}{b}(E_1 \otimes E_{DR})W + \frac{1}{a}(E_2 \otimes D_R)W = \frac{1}{b}(E_6 \otimes E_{DR})W + \frac{1}{a}(E_7 \otimes D_R)W$$

$$= \frac{1}{a}(E_3 \otimes D_R)W + \frac{\nu_1}{b}(E_4 \otimes E_{DR})W = \frac{1}{a}(E_8 \otimes D_R)W + \frac{\nu_1}{b}(E_9 \otimes E_{DR})W$$

$$= \frac{1}{b}(E_3 \otimes E_{DR})W + \frac{1}{a}(E_4 \otimes D_R)W = \frac{1}{b}(E_8 \otimes E_{DR})W + \frac{1}{a}(E_9 \otimes D_R)W \qquad \text{(B.2)}$$

$$= \left(\kappa^2 G_1 h_1 + \kappa^2 G_2 h_2 + G_c h\right)\frac{2h}{a}(E_5 \otimes D_R)W - \kappa^2 G_1 h_1 (E_3 \otimes E_R)W$$

$$-\kappa^2 G_2 h_2 (E_8 \otimes E_R)W + G_c h(E_6 \otimes E_R)W - G_c h(E_1 \otimes E_R)W$$

$$+\frac{G_c h_2}{2}(E_8 \otimes E_R)W + \frac{G_c h_1}{2}(E_3 \otimes E_R)W = 0$$

At $x_2 = 0$

$$\frac{1}{b}(E_1 \otimes E_{DB})W + \frac{1}{a}(E_2 \otimes D_B)W = \frac{1}{b}(E_6 \otimes E_{DB})W + \frac{1}{a}(E_7 \otimes D_B)W$$

$$= \frac{1}{b}(E_2 \otimes E_{DB})W + \frac{\nu_1}{a}(E_1 \otimes D_B)W = \frac{1}{b}(E_7 \otimes E_{DB})W + \frac{\nu_1}{a}(E_6 \otimes D_B)W$$

$$= \frac{1}{b}(E_3 \otimes E_{DB})W + \frac{1}{a}(E_4 \otimes D_B)W = \frac{1}{b}(E_8 \otimes E_{DB})W + \frac{1}{a}(E_9 \otimes D_B)W$$

$$= \frac{1}{b}(E_4 \otimes E_{DB})W + \frac{\nu_1}{a}(E_3 \otimes D_B)W = \frac{1}{b}(E_9 \otimes E_{DB})W + \frac{\nu_1}{a}(E_8 \otimes D_B)W \qquad \text{(B.3)}$$

$$= \left(\kappa^2 G_1 h_1 + \kappa^2 G_2 h_2 + G_c h\right)\frac{2h}{b}(E_5 \otimes E_{DB})W - \kappa^2 G_1 h_1 (E_4 \otimes E_B)W$$

$$-\kappa^2 G_2 h_2 (E_9 \otimes E_B)W + G_c h(E_7 \otimes E_B)W - G_c h(E_6 \otimes E_B)W$$

$$+\frac{G_c h_2}{2}(E_9 \otimes E_B)W + \frac{G_c h_1}{2}(E_4 \otimes E_B)W = 0$$

At $x_2 = b$

$$\frac{1}{b}(E_1 \otimes E_{DT})W + \frac{1}{a}(E_2 \otimes D_T)W = \frac{1}{b}(E_6 \otimes E_{DT})W + \frac{1}{a}(E_7 \otimes D_T)W$$

$$= \frac{1}{b}(E_2 \otimes E_{DT})W + \frac{\nu_1}{a}(E_1 \otimes D_T)W = \frac{1}{b}(E_7 \otimes E_{DT})W + \frac{\nu_1}{a}(E_6 \otimes D_T)W$$

$$= \frac{1}{b}(E_3 \otimes E_{DT})W + \frac{1}{a}(E_4 \otimes D_T)W = \frac{1}{b}(E_8 \otimes E_{DT})W + \frac{1}{a}(E_9 \otimes D_T)W$$

$$= \frac{1}{b}(E_4 \otimes E_{DT})W + \frac{\nu_1}{a}(E_3 \otimes D_T)W = \frac{1}{b}(E_9 \otimes E_{DT})W + \frac{\nu_1}{a}(E_8 \otimes D_T)W \qquad \text{(B.4)}$$

$$= \left(\kappa^2 G_1 h_1 + \kappa^2 G_2 h_2 + G_c h\right)\frac{2h}{b}(E_5 \otimes E_{DT})W - \kappa^2 G_1 h_1 (E_4 \otimes E_T)W$$

$$-\kappa^2 G_2 h_2 (E_9 \otimes E_T)W + G_c h(E_7 \otimes E_T)W - G_c h(E_6 \otimes E_T)W$$

$$+\frac{G_c h_2}{2}(E_9 \otimes E_T)W + \frac{G_c h_1}{2}(E_4 \otimes E_T)W = 0$$

where $D_R = D_1(1,:) \otimes E$; $D_B = D_1 \otimes E(M+1,:)$; $D_T = D_1 \otimes E(1,:)$; $E_{DR} = E(1,:) \otimes D_1$; $E_{DB} = E \otimes D_1(M+1,:)$; $E_{DT} = E \otimes D_1(1,:)$.

References

[1] Ferry JD. Viscoelastic properties of polymers. John Wiley & Sons; 1980.
[2] Sayyad AS, Ghugal YM. On the free vibration analysis of laminated composite and sandwich plates: a review of recent literature with some numerical results. Compos Struct 2015;129:177–201. https://doi.org/10.1016/j.compstruct.2015.04.007.
[3] Abrate S, Di Sciuva M. Equivalent single layer theories for composite and sandwich structures: a review. Compos Struct 2017;179:482–94. https://doi.org/10.1016/j.compstruct.2017.07.090.
[4] Tossapanon P, Wattanasakulpong N. Stability and free vibration of functionally graded sandwich beams resting on two-parameter elastic foundation. Compos Struct 2016;142:215–25. https://doi.org/10.1016/j.compstruct.2016.01.085.
[5] Tossapanon P, Wattanasakulpong N. Flexural vibration analysis of functionally graded sandwich plates resting on elastic foundation with arbitrary boundary conditions: chebyshev collocation technique. J Sandw Struct Mater 2020;22(2):156–89. https://doi.org/10.1177/1099636217736003.
[6] Carrera E. Historical review of zig-zag theories for multilayered plates and shells. Appl Mech Rev 2003;56(3):287–308. https://doi.org/10.1115/1.1557614.
[7] Reddy JN. On the generalization of displacement-based laminate theories. Appl Mech Rev 1989;42(11S):S213–22. https://doi.org/10.1115/1.3152393.
[8] Reddy JN. An evaluation of equivalent-single-layer and layerwise theories of composite laminates. Compos Struct 1993;25(1–4):21–35. https://doi.org/10.1016/0263-8223(93)90147-I.
[9] Liew KM, Pan ZZ, Zhang LW. An overview of layerwise theories for composite laminates and structures: development, numerical implementation and application. Compos Struct 2019;216:240–59. https://doi.org/10.1016/j.compstruct.2019.02.074.
[10] Di Sciuva M. Development of an anisotropic, multilayered, shear-deformable rectangular plate element. Comput Struct 1985;21(4):789–96. https://doi.org/10.1016/0045-7949(85)90155-5.
[11] Di Sciuva M. Bending, vibration and buckling of simply supported thick multilayered orthotropic plates: an evaluation of a new displacement model. J Sound Vib 1986;105(3):425–42. https://doi.org/10.1016/0022-460X(86)90169-0.
[12] Cho KN, Bert CW, Striz AG. Free vibrations of laminated rectangular plates analyzed by higher order individual-layer theory. J Sound Vib 1991;145(3):429–42. https://doi.org/10.1016/0022-460X(91)90112-W.

[13] Lu X, Liu D. An interlaminar shear stress continuity theory for both thin and thick composite laminates. J Appl Mech 1992;59(3):502–9. https://doi.org/10.1115/1.2893752.

[14] Robbins Jr DH, Reddy JN. Modelling of thick composites using a layerwise laminate theory. Int J Numer Meth Eng 1993;36(4):655–77. https://doi.org/10.1002/nme.1620360407.

[15] Carrera E. Mixed layer-wise models for multilayered plates analysis. Compos Struct 1998;43(1):57–70. https://doi.org/10.1016/S0263-8223(98)00097-X.

[16] Wang G, Veeramani S, Wereley NM. Analysis of sandwich plates with isotropic face plates and a viscoelastic core. J Vib Acoust 2000;122(3):305–12. https://doi.org/10.1115/1.1303065.

[17] Rao MK, Scherbatiuk K, Desai YM, et al. Natural vibrations of laminated and sandwich plates. J Eng Mech 2004;130(11):1268–78. https://doi.org/10.1061/(ASCE)0733-9399(2004)130:11(1268).

[18] Ferreira AJM, Fasshauer GE, Batra RC, et al. Static deformations and vibration analysis of composite and sandwich plates using a layerwise theory and RBF-PS discretizations with optimal shape parameter. Compos Struct 2008;86(4):328–43. https://doi.org/10.1016/j.compstruct.2008.07.025.

[19] Fares ME, Elmarghany MK. A refined zigzag nonlinear first-order shear deformation theory of composite laminated plates. Compos Struct 2008;82(1):71–83. https://doi.org/10.1016/j.compstruct.2006.12.007.

[20] Plagianakos TS, Saravanos DA. Higher-order layerwise laminate theory for the prediction of interlaminar shear stresses in thick composite and sandwich composite plates. Compos Struct 2009;87(1):23–35. https://doi.org/10.1016/j.compstruct.2007.12.002.

[21] Ćetković M, Vuksanović DJ. Bending, free vibrations and buckling of laminated composite and sandwich plates using a layerwise displacement model. Compos Struct 2009;88(2):219–27. https://doi.org/10.1016/j.compstruct.2008.03.039.

[22] Li D, Liu Y, Zhang X. A layerwise/solid-element method of the linear static and free vibration analysis for the composite sandwich plates. Compos B Eng 2013;52:187–98. https://doi.org/10.1016/j.compositesb.2013.04.031.

[23] Bilasse M, Oguamanam DCD. Forced harmonic response of sandwich plates with viscoelastic core using reduced-order model. Compos Struct 2013;105:311–8. https://doi.org/10.1016/j.compstruct.2013.05.042.

[24] Maturi DA, Ferreira AJM, Zenkour AM, et al. Analysis of sandwich plates with a new layerwise formulation. Compos B Eng 2014;56:484–9. https://doi.org/10.1016/j.compositesb.2013.08.086.

[25] Pandey S, Pradyumna S. A new C^0 higher-order layerwise finite element formulation for the analysis of laminated and sandwich plates. Compos Struct 2015;131:1–16. https://doi.org/10.1016/j.compstruct.2015.04.034.

[26] Liu N, Jeffers AE. Isogeometric analysis of laminated composite and functionally graded sandwich plates based on a layerwise displacement theory. Compos Struct 2017;176:143–53. https://doi.org/10.1016/j.compstruct.2017.05.037.

[27] Zhao R, Yu K, Hulbert GM, et al. Piecewise shear deformation theory and finite element formulation for vibration analysis of laminated composite and sandwich plates in thermal environments. Compos Struct 2017;160:1060–83. https://doi.org/10.1016/j.compstruct.2016.10.103.

[28] Hashin Z. Complex moduli of viscoelastic composites—I. General theory and application to particulate composites. Int J Solids Struct 1970;6(5):539–52. https://doi.org/10.1016/0020-7683(70)90029-6.

[29] Chinnaboon B, Panyatong M, Chucheepsakul S. Orthotropic plates resting on viscoelastic foundations with a fractional derivative kelvin-voigt model. Compos Struct 2023;322:117400. https://doi.org/10.1016/j.compstruct.2023.117400.

[30] Permoon MR, Farsadi T. Free vibration of three-layer sandwich plate with viscoelastic core modelled with fractional theory. Mech Res Commun 2021;116:103766. https://doi.org/10.1016/j.mechrescom.2021.103766.

[31] D'ottavio M, Krasnobrizha A, Valot E, et al. Dynamic response of viscoelastic multiple-core sandwich structures. J Sound Vib 2021;491:115753. https://doi.org/10.1016/j.jsv.2020.115753.

[32] Bagley RL, Torvik PJ. Fractional calculus-a different approach to the analysis of viscoelastically damped structures. AIAA J 1983;21(5):741–8. https://doi.org/10.2514/3.8142.

[33] Golla DF, Hughes PC. Dynamics of viscoelastic structures—a time-domain, finite element formulation. J Appl Mech 1985;52(4):897–906. https://doi.org/10.1115/1.3169166.

[34] McTavish D, Hughes P. Finite element modeling of linear viscoelastic structures-the GHM method, 33rd Structures, Structural Dynamics and Materials Conference, 1992: 2380. Doi: 10.2514/6.1992-2380.

[35] Lesieutre GA, Mingori DL. Finite element modeling of frequency-dependent material damping using augmenting thermodynamic fields. J Guid Control Dynam 1990;13(6):1040–50. https://doi.org/10.2514/3.20577.

[36] Lesieutre GA, Bianchini E. Time domain modeling of linear viscoelasticity using anelastic displacement fields. J Vib Acoust 1995;117(4):424–30. https://doi.org/10.1115/1.2874474.

[37] Nashif AD, Jones DIG, Henderson JP. Vibration damping. John Wiley & Sons; 1991.

[38] American Society for Testing and Materials. Standard test method for measuring vibration-damping properties of materials. ASTM International, 2010.

[39] Trefethen LN. Spectral methods in MATLAB. Society for Industrial and Applied Mathematics 2000.

[40] Malik MR, Zang TA, Hussaini MY. A spectral collocation method for the Navier-Stokes equations. J Comput Phys 1985;61(1):64–88. https://doi.org/10.1016/0021-9991(85)90061-0.

[41] Makinde OD. On the chebyshev collocation spectral approach to stability of fluid flow in a porous medium. Int J Numer Meth Fluids 2009;59(7):791–9. https://doi.org/10.1002/fld.1847.

[42] Subich CJ, Lamb KG, Stastna M. Simulation of the navier-stokes equations in three dimensions with a spectral collocation method. Int J Numer Meth Fluids 2013;73(2):103–29. https://doi.org/10.1002/fld.3788.

[43] Sun J, Kari L, Arteaga IL. A dynamic rotating blade model at an arbitrary stagger angle based on classical plate theory and the Hamilton's principle. J Sound Vib 2013;332(5):1355–71. https://doi.org/10.1016/j.jsv.2012.10.030.

[44] Quintanilla FH, Lowe MJS, Craster RV. Modeling guided elastic waves in generally anisotropic media using a spectral collocation method. J Acoust Soc Am 2015;137(3):1180–94. https://doi.org/10.1121/1.4913777.

[45] Ji M, Inaba K. Theoretical analysis of free vibration and transient response of rectangular plate–cavity system under impact loading. J Press Vessel Technol 2023;145(3):031402. https://doi.org/10.1115/1.4062121.

[46] Ji M, Sekiguchi Y, Inaba K, et al. Forward and inverse analysis of transient responses for a cantilevered rectangular plate under normal and oblique impact loadings. Int J Impact Eng 2023;174:104514. https://doi.org/10.1016/j.ijimpeng.2023.104514.

[47] Ji M, Inaba K, Triawan F. Vibration characteristics of cylindrical shells filled with fluid based on first-order shell theory. J Fluids Struct 2019;85:275–91. https://doi.org/10.1016/j.jfluidstructs.2019.01.017.

[48] Ji M, Wu YC, Ma CC. Analytical solutions for in-plane dominated vibrations of transversely isotropic circular plates based on high-order theories. J Sound Vib 2021;503:116110. https://doi.org/10.1016/j.jsv.2021.116110.

[49] Ji M, Wu YC, Ma CC. Theoretical analyses and numerical simulation of flexural vibration based on Reddy and modified higher-order plate theories for a transversely isotropic circular plate. Acta Mech 2021;232:2825–42. https://doi.org/10.1007/s00707-021-02973-y.

[50] Ji M, Wu YC, Ma CC. In-plane-dominated vibration characteristics of piezoelectric thick circular plates based on higher-order plate theories. J Mech 2022;38:410–32. https://doi.org/10.1093/jom/ufac034.

[51] Cheynet E, Daniotti N, Jakobsen JB, et al. Improved long-span bridge modeling using data-driven identification of vehicle-induced vibrations. Struct Control Health Monit 2020;27(9):e2574.

[52] Graesser EJ, Wong CR. The relationship of traditional damping measures for materials with high damping capacity: a review. ASTM International; 1992.

[53] Liu W. Experimental and analytical estimation of damping in beams and plates with damping treatments. University of Kansas; 2008. Doctoral dissertation.

[54] Xu X. Machine learning approach to characterize elastic, viscoelastic, relaxation and creep behavior of materials. Tandon School of Engineering, New York University; 2020. Doctoral dissertation.

[55] https://multimedia.3m.com/mws/media/307979O/3mtm-ultra-pure-viscoelastics-damping-polymer-242nr02.pdf.